

Rochester Institute of Technology

**RIT Scholar Works**

---

Theses

---

1-2015

## **Performance and Energy Trade-offs for 3D IC NoC Interconnects and Architectures**

James David Coddington

Follow this and additional works at: <https://scholarworks.rit.edu/theses>

---

### **Recommended Citation**

Coddington, James David, "Performance and Energy Trade-offs for 3D IC NoC Interconnects and Architectures" (2015). Thesis. Rochester Institute of Technology. Accessed from

This Thesis is brought to you for free and open access by RIT Scholar Works. It has been accepted for inclusion in Theses by an authorized administrator of RIT Scholar Works. For more information, please contact [ritscholarworks@rit.edu](mailto:ritscholarworks@rit.edu).

# **Performance and Energy Trade-offs for 3D IC NoC**

## **Interconnects and Architectures**

by

**James David Coddington**

A Thesis Submitted in Partial Fulfillment of the Requirements for the Degree of  
Master of Science in Computer Engineering

Supervised by

Dr. Amlan Ganguly  
Department of Computer Engineering  
Kate Gleason College of Engineering  
Rochester Institute of Technology  
Rochester, NY  
January, 2015

### **Approved By:**

---

Dr. Amlan Ganguly  
*Primary Advisor – R.I.T. Dept. of Computer Engineering*

---

Dr. Andres Kwasinski  
*Secondary Advisor – R.I.T. Dept. of Computer Engineering*

---

Dr. Juan Cockburn  
*Secondary Advisor – R.I.T. Dept. of Computer Engineering*

# Dedication

I would like to dedicate this thesis to my wife Gwenlyn and my parents Dave and Kim Coddington. They have been consistently supporting me throughout my academic career and without them, none of this would be possible.

# Acknowledgements

I'd like to thank my advisor, Dr. Amlan Ganguly for his expertise and help throughout my graduate research. I'd also like to thank my committee members Dr. Juan Cockburn and Dr. Andres Kwasinski for their constructive feedback and professional opinions. Lastly, I'd like to thank Shahriar Shamim for his help getting started with the network-on-chip simulator.

## **Abstract**

With the increased complexity and continual scaling of integrated circuit performance, multi-core chips with dozens, hundreds, even thousands of parallel computing units require high performance interconnects to maximize data throughput and minimize latency and energy consumption. High core counts render bus based interconnects inefficient and lackluster in performance. Networks-on-Chip were introduced to simplify the interconnect design process and maintain a more scalable interconnection architecture. With the continual scaling of feature sizes for smaller and smaller transistors, the global interconnections of planar integrated circuits are consuming higher energy proportional to the rest of the chip power dissipation as well as increasing communication delays. Three-dimensional integrated circuits were introduced to shorten global wire lengths and increase chip connectivity. These 3D ICs bring heat dissipation challenges as the power density increases drastically for each additional chip layer. One of the most popularly researched vertical interconnection technologies is through-silicon vias (TSVs). TSVs require additional manufacturing steps to build but generally have low energy dissipation and good performance. Alternative wireless technologies such as capacitive or inductive coupling do not require additional manufacturing steps and also provide the option of having a liquid cooling layer between planar chips. They are typically much slower and consume more energy than their wired counterparts, however. This work compares the interconnection technologies across several different NoC architectures including a proposed sparse 3D mesh for inductive coupling that increases vertical throughput per link and reduces chip area compared to the other wireless architectures and technologies.

# Table of Contents

Dedication .....	ii
Acknowledgements .....	iii
Abstract .....	iv
Table of Contents .....	v
List of Figures .....	viii
List of Tables .....	xi
Chapter 1 Introduction .....	1
1.1. From Single to Multi-Processor Systems .....	1
1.2. Network-on-Chip Data Routing .....	2
1.3. To The Third Dimension .....	3
1.4. Thesis Contributions .....	4
Chapter 2 Related Work .....	6
2.1. 3D ICs .....	6
2.2. 3D Wired NoCs .....	6
2.3. 3D Wireless NoCs .....	7
2.4. Emerging Technologies .....	7
Chapter 3 Wired 3D NoC Architectures .....	9
3.1. Dense 3D Mesh NoC .....	9
3.2. Performance Metrics .....	10

3.3.	NoC Performance Evaluation .....	11
3.3.1	Bandwidth .....	12
3.3.2	Energy per Message .....	13
3.3.3	Network Latency .....	14
3.4.	NoC Performance Evaluation with Non-Uniform Traffic.....	15
3.4.1	Energy per Message .....	15
3.4.2	Network Latency .....	17
3.5.	TSV Density Analysis .....	17
3.5.1	NoC Performance Evaluation.....	18
3.5.2	NoC Performance Evaluation with Non-Uniform Traffic .....	23
3.6.	Area Overheads .....	27
Chapter 4	Wireless 3D NoC Architectures .....	28
4.1.	Performance Evaluation .....	30
4.1.1	Bandwidth .....	30
4.1.2	Energy per Message .....	32
4.1.3	Latency .....	35
4.2.	Performance Evaluation with Non-Uniform Traffic .....	36
4.2.1	Energy per Message .....	37
4.2.2	Latency .....	39
4.3.	Area Overheads .....	40

Chapter 5	Conclusions .....	42
5.1.	Summary.....	42
5.1.1	System Bandwidth.....	42
5.1.2	System Energy per Message .....	43
5.1.3	System Latency .....	46
5.1.4	Chip Area .....	49
5.1.5	Overall.....	50
5.2.	Future Work.....	50
References	.....	52



## List of Figures

Figure 1-1: 16 Core 2D Mesh Network-on-Chip.....	2
Figure 3-1: One Plane of a Dense 3D Mesh .....	9
Figure 3-2: 3D Connections for a Dense 3D Mesh.....	9
Figure 3-3: TSV Uniform Traffic Peak Bandwidth.....	12
Figure 3-4: TSV Uniform Traffic Energy per Message.....	13
Figure 3-5: TSV Uniform Traffic Energy per Message without Waiting .....	14
Figure 3-6: TSV Uniform Traffic Average Latency.....	15
Figure 3-7: TSV Non-Uniform Traffic Energy per Message .....	16
Figure 3-8: TSV Non-Uniform Traffic Energy per Message without Waiting ....	16
Figure 3-9: TSV Non-Uniform Traffic Average Latency.....	17
Figure 3-10: TSV Density Analysis with 32 bits/flit Uniform Traffic Peak Bandwidth.....	19
Figure 3-11: TSV Density Analysis with 64 bits/flit Uniform Traffic Peak Bandwidth.....	19
Figure 3-12: TSV Density Analysis with an 8x4x8 NoC and 32 bits/flit Uniform Traffic .....	20
Figure 3-13: TSV Density Analysis with an 8x8x8 NoC and 32 bits/flit Uniform Traffic .....	20
Figure 3-14: TSV Density Analysis with 32 bits/flit Uniform Traffic Energy per Message.....	21
Figure 3-15: TSV Density Analysis with 64 bits/flit Uniform Traffic Energy per Message.....	21

Figure 3-16: TSV Density Analysis with 32 bits/flit Uniform Traffic Energy per Message without Waiting .....	22
Figure 3-17: TSV Density Analysis with 64 bits/flit Uniform Traffic Energy per Message without Waiting .....	22
Figure 3-18: TSV Density Analysis with 32 bits/flit Uniform Traffic Average Latency.....	23
Figure 3-19: TSV Density Analysis with 64 bits/flit Uniform Traffic Average Latency.....	23
Figure 3-20: TSV Density Analysis with 32 bits/flit Non-Uniform Traffic Energy per Message .....	24
Figure 3-21: TSV Density Analysis with 64 bits/flit Non-Uniform Traffic Energy per Message .....	24
Figure 3-22: TSV Density Analysis with 32 bits/flit Non-Uniform Traffic Energy per Message without Waiting .....	25
Figure 3-23: TSV Density Analysis with 64 bits/flit Non-Uniform Traffic Energy per Message without Waiting .....	25
Figure 3-24: TSV Density Analysis with 32 bits/flit Non-Uniform Traffic Average Latency.....	26
Figure 3-25: TSV Density Analysis with 64 bits/flit Non-Uniform Traffic Average Latency.....	26
Figure 4-1: 3D Ring NoC .....	29
Figure 4-2: Inductive Coupling Sparse 3D Mesh NoC.....	29

Figure 4-3: Wireless Comparison with 32 bits/flit Uniform Traffic Peak Bandwidth.....	31
Figure 4-4: Wireless Comparison with 64 bits/flit Uniform Traffic Peak Bandwidth.....	31
Figure 4-5: Wireless Comparison with 32 bits/flit Uniform Traffic Energy per Message.....	33
Figure 4-6: Wireless Comparison with 64 bits/flit Uniform Traffic Energy per Message.....	34
Figure 4-7: Wireless Comparison with 32 bits/flit Uniform Traffic Energy per Message without Waiting .....	35
Figure 4-8: Wireless Comparison with 64 bits/flit Uniform Traffic Energy per Message without Waiting .....	35
Figure 4-9: Wireless Comparison with 32 bits/flit Uniform Traffic Average Latency.....	36
Figure 4-10: Wireless Comparison with 64 bits/flit Uniform Traffic Average Latency.....	36
Figure 4-11: Wireless Comparison with 32 bits/flit Non-Uniform Traffic Energy per Message .....	37
Figure 4-12: Wireless Comparison with 64 bits/flit Non-Uniform Traffic Energy per Message .....	38
Figure 4-13: Wireless Comparison with 32 bits/flit Non-Uniform Traffic Energy per Message without Waiting .....	38

Figure 4-14: Wireless Comparison with 64 bits/flit Non-Uniform Traffic Energy per Message without Waiting .....	39
Figure 4-15: Wireless Comparison with 32 bits/flit Non-Uniform Traffic Average Latency.....	40
Figure 4-16: Wireless Comparison with 64 bits/flit Non-Uniform Traffic Average Latency.....	40

## List of Tables

Table 4-1: Technology and Architecture Pairs System Average Hop Count Comparison.....	31
Table 4-2: Technology and Architecture Pairs 32 bits/flit System Bandwidth Comparison.....	32
Table 4-3: Technology and Architecture Pairs 64 bits/flit System Bandwidth Comparison.....	32
Table 4-4: Technology and Architecture Pairs System Chip Area Overhead Comparison.....	41

# Chapter 1 Introduction

In recent years, the technological advancements in the production of large scale integrated circuits have been accelerating at a rapid pace and because of this, chip designers are getting closer and closer to regularly utilizing tens of billions of transistors on a single chip. Engineers are pressed with designing ever more efficient and powerful processors to perform tasks for fields that range from consumer level electronics devices to supercomputing workloads such as astrophysics, pollution and weather forecasting and modeling, fluid dynamics, and bioinformatics.

## **1.1. From Single to Multi-Processor Systems**

For a considerable period of time in the electronics industry, it was sufficient to simply increase the operating frequency to get a considerable increase in performance. Recently, however, clock speed increases have slowed substantially due to high power dissipation from the increased switching activity density of the transistors. It is becoming increasingly difficult to remove all of the excess heat from the chip. This power restraint has shifted the design paradigm from single core processors to multicore processors and has unleashed several new challenges for chip designers [1]. Multicore processors enabled designers to utilize the additional transistors to increase performance with the addition of core-level parallelism.

One of the most difficult challenges for multi-processor systems is how to connect the individual cores to each other without limiting the performance. Some of the first multicore processors utilized a shared bus for communication between the cores. As the number of cores has increased, global interconnects that span the majority of the chip

have come to establish themselves as a limiting factor in the performance of a system [2]. In response, systems have been moving from shared-bus based architectures with longer wires to scalable Network-on-Chip (NoC) architectures with shorter wires to handle the increased communication demands for many-core chips [3]. An example 16 core 2D mesh NoC is shown in Figure 1-1. This figure shows how packets must go through at least six hops to go from one corner of the chip to the opposite corner. As more and more cores are added to the system, communication performance for data traveling from one end of the chip to the other degrades due to the increased number of cycles it takes for a packet to move through the network to its destination, even with a scalable NoC.

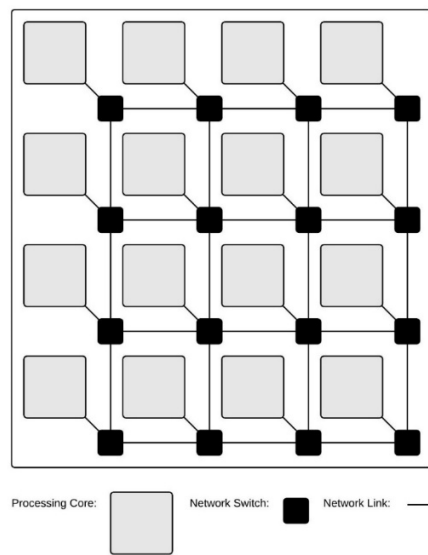


*Figure 1-1: 16 Core 2D Mesh Network-on-Chip*

## **1.2. Network-on-Chip Data Routing**

For routing data between cores in a NoC, there are conventionally three options: circuit switching, packet switching, and wormhole routing. Circuit switching reserves a path from the sending node to the receiving node to send the data. This prevents other data transmissions from using the same path at the same time and can be inefficient.

Packet switching breaks the data into packets where each packet is sent over the network separately. This requires the entire packet to be buffered at each intermediate node and takes considerable chip area to implement. One of the more popular routing schemes for NoCs is wormhole routing where a data packet that needs to be transferred from one part of the chip to another is broken into smaller flow control units called flits. The header flit contains all of the routing information and is sent first, reserving the path for the rest of the flits to follow [3]. Similar to circuit switching, wormhole routing reserves paths such that multiple packets cannot be sent through a single switch at the same time. To get passed this, virtual channels separate the packets so that more of the network capacity can be utilized. Wormhole routing is more commonly used in systems where chip area overheads are important and is utilized in this work.

### ***1.3. To The Third Dimension***

As the chip dimensions and number of cores continue to grow, the global interconnect wires continue to get longer and their relative performance degrades compared to the speed increases of transistors. In an effort to reduce the number of clock cycles it takes for packets to traverse the NoC and get further performance increases, 3D integrated circuits (3D ICs) have emerged as a viable method of shrinking the communication distances and allowing the NoC to have a higher connectivity [4]. The shorter distances and higher connectivity both contribute to higher performance. Although the overall wire lengths are reduced by switching to 3D ICs, the power density is increased significantly. The number of transistors per square millimeter increases substantially with each IC layer. This leads to higher heat dissipation, which needs to be dealt with in the design stage. The vertical connection technology and the vertical

network topology play an important role in the NoC performance and energy consumption and need to be evaluated. Several technologies have evolved into viable solutions for transferring data between the layers in the 3D ICs including Through Silicon Vias (TSVs), capacitive coupling circuits, and inductive coupling circuits. Each technology has its own distinct advantages and disadvantages which will be explored in more detail in 0 and 0.

#### **1.4. Thesis Contributions**

In this work, a comparative analysis of several vertical interconnect technologies and 3D-NoC architectures is performed. This includes a comparison of TSV, inductive coupling, and capacitive coupling based vertical interconnects in addition to the impact that TSV density has on network performance and energy consumption. It also includes a comparison of inductive coupling dense 3D mesh and ring networks to a proposed novel sparse 3D mesh architecture. This architecture is designed to reduce chip area overhead, latency, and the energy per message while minimizing the impact to the overall throughput of the network. To accomplish this, the delay and power of vertical interconnections for TSV, inductive coupling, and capacitive coupling technologies are modeled, a novel inductive coupling 3D-NoC architecture is proposed, and a 3D-NoC cycle accurate simulator is developed. The simulator is used to run simulations with various types of network traffics and benchmarks to be able to compare the different technologies and network architectures. Simulation parameters including core count, packet size, and network traffic patterns will be varied to find differences in the energy dissipation per message, the bandwidth of the system, and the average latency of the network. This is summarized in the following points:



- Delay and Power Modeling
  - TSV Delay and Power Modeling for Various TSV Densities
  - Inductive Coupling Delay and Power Modeling
  - Capacitive Coupling Delay and Power Modeling
- Architecture Comparisons
  - TSV Dense 3D Mesh
  - Inductive Coupling Dense 3D Mesh
  - Inductive Coupling Two-Way Ring
  - Inductive Coupling Sparse Mesh
  - Capacitive Coupling Dense Mesh
- Simulator Framework
  - Cycle Accurate Simulator for 3D NoCs with 3-Stage Switches
    - Input Arbitration
    - Output Arbitration
    - Routing
  - Experimental Results for the Various 3D Technologies and Architectures
    - Peak Bandwidth
    - Energy Dissipated Per Message
    - Latency
    - Non-Uniform and Uniform Traffic Patterns
    - Scalability with Respect to Increasing Message Size and Core Count

## **Chapter 2    Related Work**

### **2.1.   3D ICs**

The problems associated with the high wiring connectivity requirements of large-scale integration circuit design is explored in [5] along with how 3D ICs increase connectivity while reducing the number of long interconnects. Similarly, the authors of [6] and [7] investigate how 3D ICs can be used to combat the growing ratio of interconnect to gate delay as feature sizes decrease. A general overview of 3D technologies and the motivations behind designing 3D integrated circuits is presented in [8]. The benefits of using a 3D NoC instead of a 2D NoC are explored by Feero and Pande [4]. Their work focused on the performance and area effects of the network architectures rather than the power and performance tradeoffs of various technologies. The effects of serialization and a general comparison between TSV, inductive coupling, and capacitive coupling are discussed in [9]. However, the authors did not investigate power consumption and the effects of the vertical connection topologies. Chip manufacturers have their choice of network architectures and vertical interconnect technologies where the impact of power, performance, and chip area overheads are important.

### **2.2.   3D Wired NoCs**

As one of the more popular vertical connection technologies, through silicon vias (TSVs) and some of their manufacturing techniques are explained in [10] along with TSV electrical characteristics extraction and modeling. TSVs add additional complexity to the

manufacturing process for 3D ICs but they tend to offer good power, performance, and chip area characteristics.

### **2.3. 3D Wireless NoCs**

In [11], a low power and high data rate inductive coupling transceiver is proposed. Inductive coupling is a vertical connection technology that does not require modifications to the manufacturing process, but the power, performance, and chip area overheads are often prohibitive to the adoption of the technology. The design and implementation of a capacitive coupling transceiver is analyzed in [12] where the power, performance, and area overheads are discussed as well as restrictions that capacitive coupling links put on how the layers of the 3D ICs are assembled. Capacitive coupling also does not require changes to the manufacturing process but limits vertical scaling to two layers placed faced to face instead of multiple layers placed face to back. It also exhibits poor power, performance, and chip area overheads relative to inductive coupling and wired techniques.

### **2.4. Emerging Technologies**

Some experimental technologies show potential for being effective at reducing energy consumption and increasing performance but are not covered in this work. One of the more promising technologies is photonic interconnects. Photonic interconnects transfer data by sending signals over optical waveguides. In [13], TSVs and a reconfigurable photonic network are utilized to reduce energy consumption while maintaining performance. Photonic interconnects have the benefit of their bandwidth being independent of the communication distance. Unfortunately, there are extra

manufacturing steps that are required to build circuits that include photonic interconnects. These extra steps add to the complexity and overall cost of these systems.

Another technology for connecting cores in a system utilizes wireless interconnects. Radio frequency transceivers can be built into the chip and used to transmit data across larger distances with less power and less latency than traditional wires. Small world networks and millimeter-wave wireless networks on chip are explored in [14] and [15]. In [16], wireless interconnects that utilize CDMA to allow multiple wireless transceivers to operate at the same time are simulated to analyze their performance and energy characteristics. Wireless interconnects can also be utilized for transferring data between layers of 3D ICs as in [17].

## Chapter 3 Wired 3D NoC Architectures

### 3.1. Dense 3D Mesh NoC

In a dense 3D mesh, each core has a switch with at most four planar connections and two vertical connections. A single layer of the dense 3D mesh network is shown in Figure 3-1. Two different sized networks are utilized in this work. A 64 core configuration made up of four planes that contain cores laid out in a four by four grid, and a 256 core configuration made up of four planes that contain cores laid out in an eight by eight grid. Each of the switches are connected in both directions vertically and in each of the four cardinal directions. An example of the 3D connections is shown in Figure 3-2.

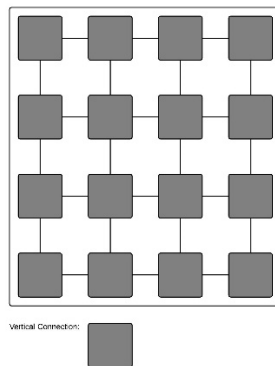


Figure 3-1: One Plane of a Dense 3D Mesh

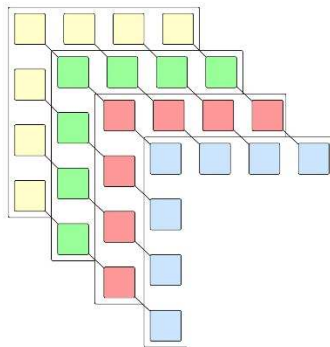


Figure 3-2: 3D Connections for a Dense 3D Mesh

### 3.2. Performance Metrics

A cycle accurate simulator implementing the dense 3D mesh architectures with core counts of 64 and 256 cores is used for the experiments. The switches are modeled with input arbitration, output arbitration, and routing stages [3]. Each switch has 8 virtual channels (VCs) to prevent deadlocking. There are 16 buffers for each switch as well as to enable switches to route multiple flits at once. Energy metrics are calculated using a 2.5 GHz global clock and all simulations are run for 5000 cycles with the energy and performance metrics starting after the 1000<sup>th</sup> cycle to allow the network to settle. Wireline links are designed to be able to transfer an entire flit in a single cycle unless the link is too long. In that case, FIFO buffers are used so that flits can be transferred between stages in a single cycle. The simulations are run both with a flit size of 32 bits and a flit size of 64 bits and all of the simulations are run with packet sizes of 64 flits. The system is designed so that there are enough wires to transmit a single flit in one cycle. With 32 bits per flit there are 32 data wires for each link and with 64 bits per flit there are 64 data wires for each network link. The wormhole routing table is constructed by using a hop based Dijkstra algorithm.

The performance metrics of interest are the bandwidth, the average energy per message, the average message latency, and the chip area overheads of the various technologies. The bandwidth of the system in bits per second can be determined as:

$$B = t \beta N f \quad (1)$$

In equation (1), the throughput,  $t$ , is the number of flits that are received per core per clock cycle when the network is saturated,  $\beta$  is the number of bits that are contained in a single flit,  $N$  is the number of cores in the system, and  $f$  is the clock frequency for the

system. The throughput is measured by the simulator. The energy per message can be calculated by:

$$E_{pkt} = \frac{\left( \sum_{i=1}^{N_{pkt}} (L_i - h_i \lambda) E_{buf} + h_i E_{wire} \lambda \right) + \lambda E_{vertical}}{N_{pkt}} \quad (2)$$

In equation (2),  $N_{pkt}$  is the number of packets that were routed during the simulation,  $L_i$  is the latency of the  $i^{\text{th}}$  packet,  $h_i$  is the number of hops that the  $i^{\text{th}}$  packet took to reach its destination,  $E_{buf}$  is the energy dissipated by the flits passing through the switch buffers,  $E_{wire}$  is the energy dissipated by the flits traveling over the planar wires,  $\lambda$  is the number of flits that are in each packet, and  $E_{vertical}$  is the energy dissipated by the flits traveling between layers of the 3D-IC. The energy per packet is tracked by the simulator. The average latency is also tracked by the simulator and is easily calculated by:

$$Latency = cycle_{absorption} - cycle_{insertion} \quad (3)$$

In equation (3) the  $cycle_{absorption}$  is the simulation cycle in which the tail flit was absorbed by the receiving core and the  $cycle_{insertion}$  is the simulation cycle in which the header flit was inserted into the network.

### 3.3. NoC Performance Evaluation

The vertical connections for these simulations utilize 32 TSVs when working with 32 bits per flit and 64 TSVs when working with 64 bits per flit. Because of its single cycle flit transmission times and low energy per bit, the dense 3D mesh with TSVs is likely to have the best performance and energy efficiency of the other technology and architecture combinations discussed later in 0. Using the  $\Pi$  model proposed in [10], a single TSV consumes 17.459 fJ/bit.

### 3.3.1 Bandwidth

The peak bandwidth for a 3D NoC that utilizes TSVs for the vertical interconnects is measured at network saturation by simulating the 3D mesh architectures of 64 cores and 256 cores. These simulations utilize uniform random traffic where each core has an equal probability to start sending a message to any other core. In Figure 3-3, the peak bandwidths for 64 and 256 core systems that utilize 32 and 64 bits per flit are shown.

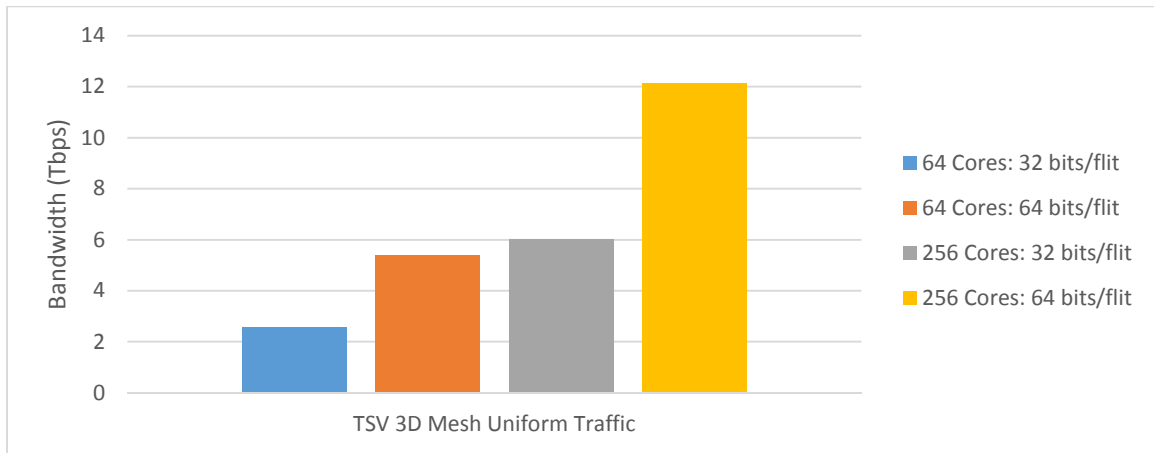


Figure 3-3: TSV Uniform Traffic Peak Bandwidth

When the system size is increased by a factor of 4, the peak bandwidth only increases by a factor of approximately 2.3. This is likely due to an increase in the average hop count when switching from the 4x4x4 to the 8x8x4 network configuration. The 64 core dense 3D mesh has an average hop count of 3.8095 while the 256 core dense 3D mesh has an average hop count of 6.5255. The higher hop count results in more of the packets reserving more of the overall network paths which reduces the peak bandwidth. However, when the number of flits is doubled the peak bandwidth also doubles. This is useful for increasing system performance but also results in higher chip area overheads



and energy dissipation. The effect that slowing down the vertical transmission times has on uniform traffic bandwidth is explored in more detail in section 3.5.1.1.

### 3.3.2 Energy per Message

The average energy per packet measurement is started a thousand cycles after the simulation begins to allow the network to settle. In Figure 3-4, the energy per message measurements for 64 and 256 core systems that use 32 and 64 bits per flit are shown.

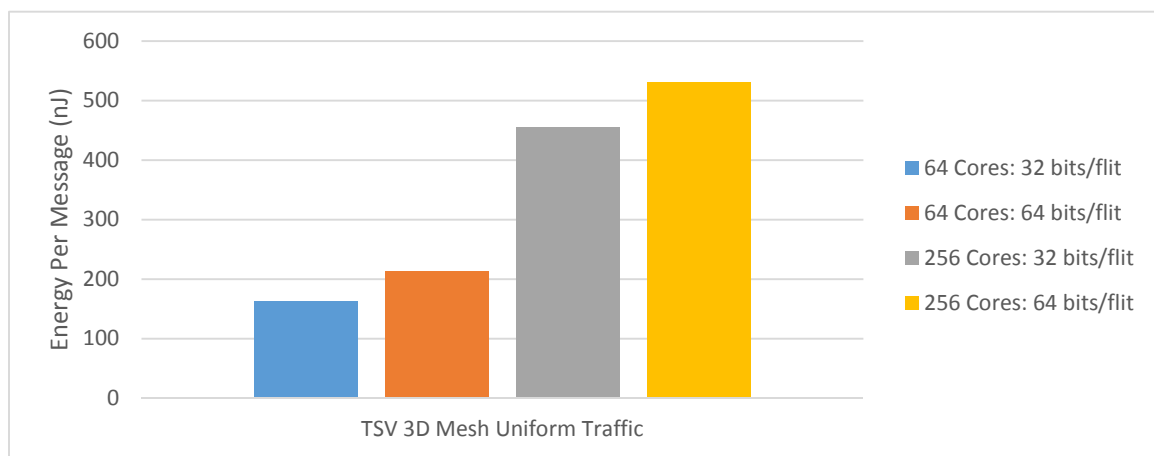


Figure 3-4: TSV Uniform Traffic Energy per Message

When the packet size is doubled from 32 to 64 bits per flit, the average energy dissipated per message only increases by 1.3 for the 64 core system and 1.2 for the 256 core system. This is a result of the increase of the energy dissipated by data transfer to energy dissipated by waiting for network links to become free ratio when going from 32 bits per flit to 64 bits per flit. The energy dissipated by the system for transferring data is shown in Figure 3-5 where the energy from waiting is removed from the overall energy measurements. When the system size increases from 64 to 256 cores, the energy increases by 2.8 for sending packets with 32 bits per flit and 2.5 for sending packets with 64 bits per flit. Similar to the bandwidth differences, this is caused by the increase in

average hop count. The high network congestion also contributes to the increased difference between the energy per message and the energy per message without waiting. The effect that slowing down the vertical transmission times has on uniform traffic energy dissipation is explored in more detail in section 3.5.1.2.

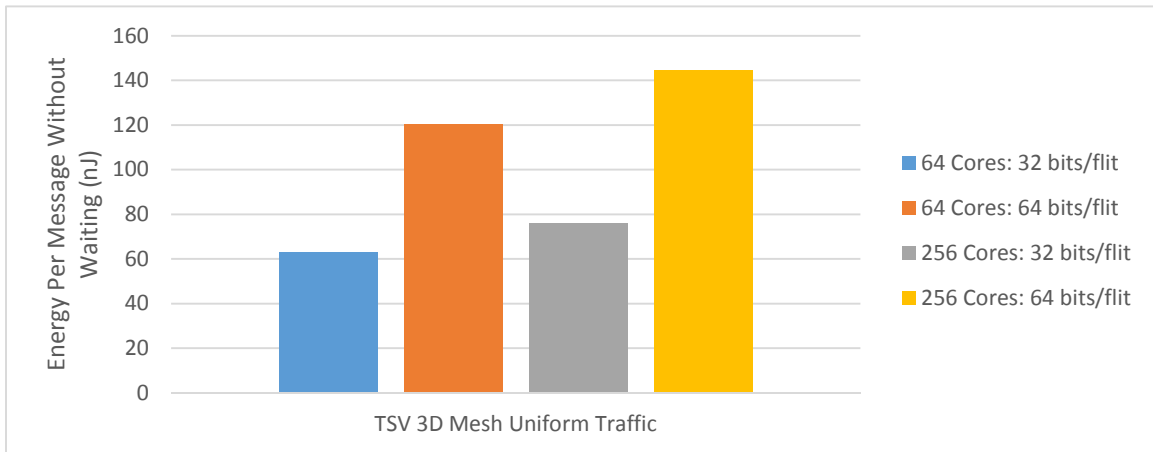


Figure 3-5: TSV Uniform Traffic Energy per Message without Waiting

### 3.3.3 Network Latency

The average latency of a message is measured after one thousand cycles to allow the network traffics to stabilize. It is calculated as the average difference between the cycle numbers that the header flits were injected into the system and the cycle numbers that the tail flits were absorbed by the destination cores. In Figure 3-6, the average network latency measurements from header flit insertion to tail flit absorption are shown. This shows an increase of a factor of 1.6 when scaling the number of cores from 64 to 256. Again, the average hop count contributes to the increased latency observed. The high network congestion also significantly affects the overall latency. The effect that decreasing the number of TSVs and slowing down the vertical transmission times has on

uniform traffic latency is explored in more detail in section 3.5.1.3.

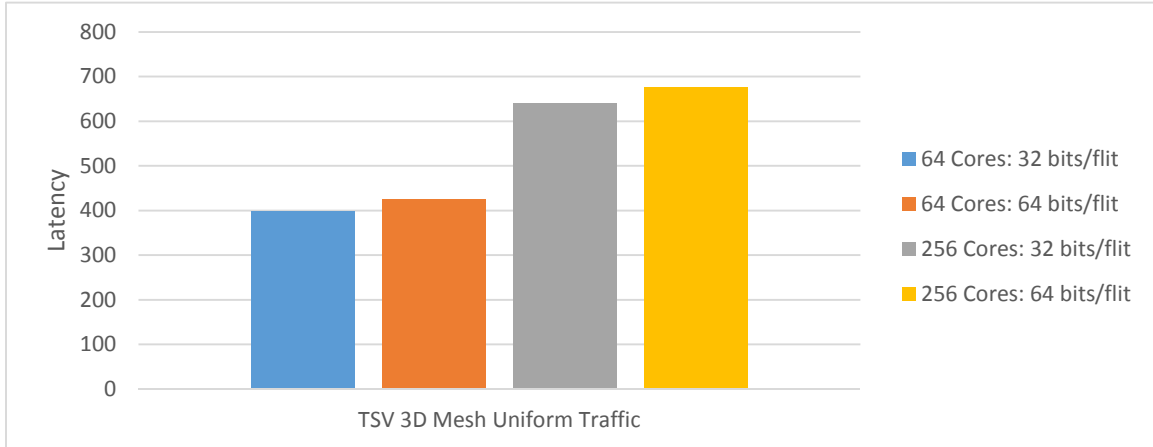


Figure 3-6: TSV Uniform Traffic Average Latency

### 3.4. NoC Performance Evaluation with Non-Uniform Traffic

Non-uniform traffic patterns utilizing 64 cores were also explored to evaluate how the network would perform with some common workloads and benchmarks. This gives a better representation of the real world characteristics of the networks. The non-uniform traffic patterns utilize extracted core to core communication frequencies for each benchmark. BODYTRACK, CANNEAL, DEDUP, FFT, FLUIDANIMATE, FREQMINE, LU, RADIX, SWAPTION, and VIPS benchmarks were used to demonstrate the network performance of computationally intensive or communication intensive workloads with the TSVs as the vertical connection technology.

#### 3.4.1 Energy per Message

Similar to the measurements in Section 3.3.2, the average energy per packet measurement is started a thousand cycles after the simulation begins to allow the network to settle. In Figure 3-7, the energy per message measurements for 64 core systems that use 32 and 64 bits per flit are shown. The average total energy dissipation from all of the

non-uniform traffic patterns doubles when shifting from 32 to 64 bits per flit as expected.

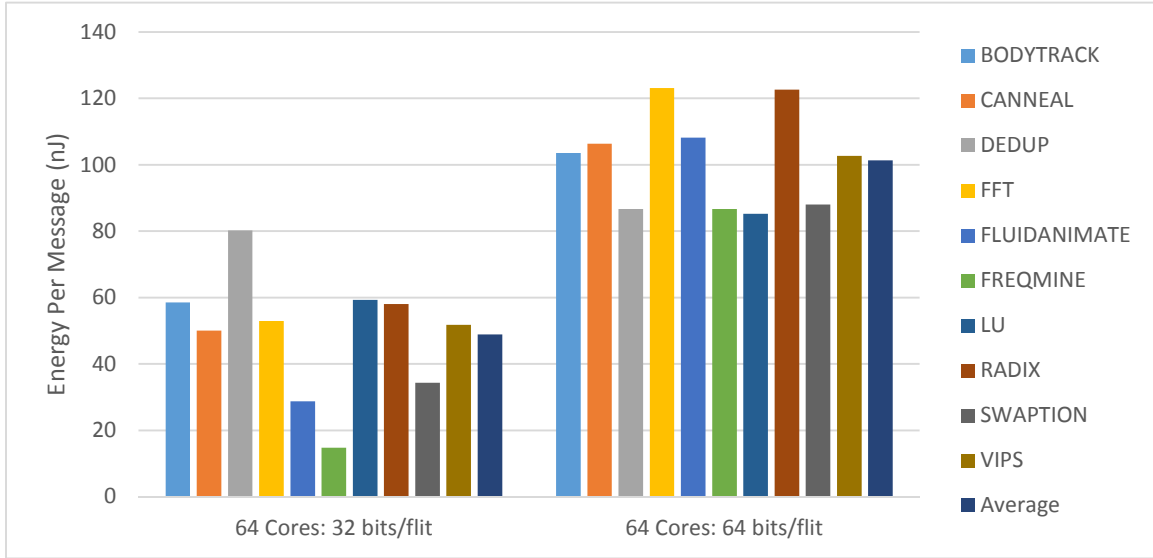


Figure 3-7: TSV Non-Uniform Traffic Energy per Message

Figure 3-8 shows the energy dissipation minus the energy used while waiting for the network links to become free. It shows that there are very few instances where the network was congested for these non-uniform traffic patterns.

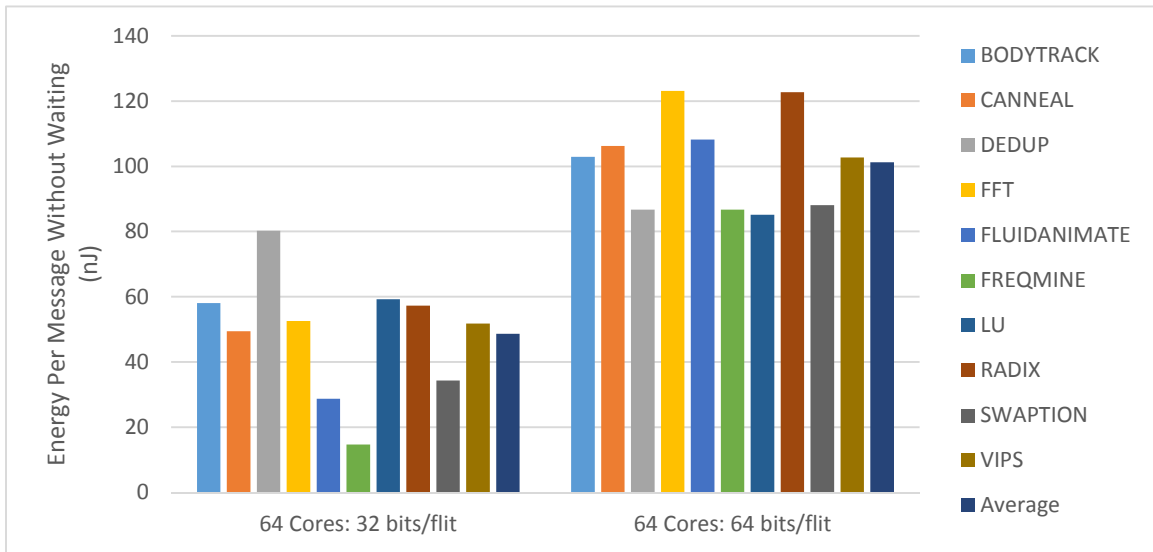


Figure 3-8: TSV Non-Uniform Traffic Energy per Message without Waiting

The energy dissipation is almost entirely from data transmission because the network spends very little time waiting for the network to be free with these traffic

patterns even with the more data intensive traffic patterns. Section 3.5.2.1 explores the effect that slowing down the vertical transmissions for non-uniform traffic patterns has on the overall energy dissipation.

### 3.4.2 Network Latency

The average latency of a message is measured after one thousand cycles to allow the network traffics to stabilize. In Figure 3-9, the average network latency measurements from header flit insertion to tail flit absorption are shown. The variation in latency between the 32 and 64 bits per flit simulations is caused by the inherent randomness in the simulations. The single cycle transmission time for all network hops enables such low latencies. The effect that slowing down the vertical transmission times for non-uniform traffic patterns has on the latency is explored in more detail in section 3.5.2.2.

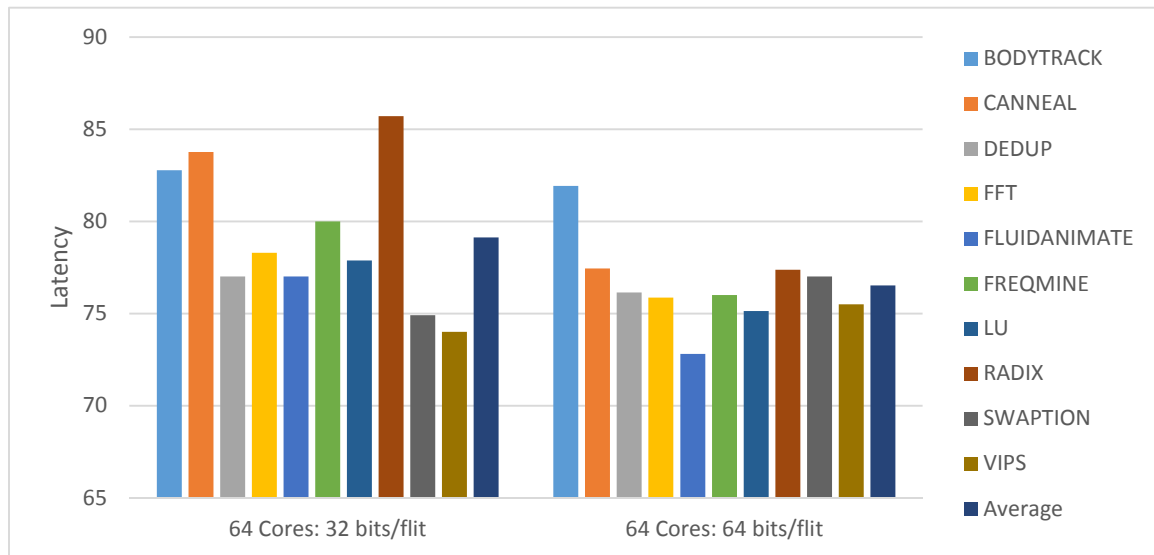


Figure 3-9: TSV Non-Uniform Traffic Average Latency

### 3.5. TSV Density Analysis

Using the electrical characteristics of TSVs from [10], the energy required to transfer a single bit through a TSV can be calculated for various pitches between the

TSVs. As the pitch between the TSVs increases, the parasitic capacitance decreases and therefore the energy required to transfer a bit is reduced. As long as the network is not saturated and flits are not consistently waiting to be routed, the number of TSVs can be reduced so that it takes multiple cycles to transmit a flit but the overall energy consumption is lower and the area overhead of the TSVs is the same. By cutting the number of TSVs per link in half, the pitch doubles, and it takes twice as long to transmit the flit through that link.

### **3.5.1 NoC Performance Evaluation**

The TSV density analysis is done by simulating the 64 and 256 core networks with enough TSVs per vertical link to transfer an entire flit in one, two, and four cycles. When working with 32 bit flits, that requires 32, 16, and 8 TSVs respectively. Likewise, with 64 bit flits, 64, 32, and 16 TSVs were used. Using the same  $\Pi$  model from [10], the full number of TSVs each use 17.459 fJ/bit again, half the number of TSVs take 9.2078 fJ/bit, while half again the number of TSVs only utilize 6.1044 fJ/bit. This shows a diminishing return in cutting the number of TSVs.

#### **3.5.1.1 Bandwidth**

The peak bandwidth for 64 and 256 core systems with increasing flit vertical transmit times is shown in Figure 3-10 and Figure 3-11. If the TSVs are designed so that they take two cycles to transmit a flit between layers, then the 64 core systems do not end up with much of a peak performance hit, which is desirable. The 256 core systems show an increase in peak bandwidth when the vertical transmit times are doubled, indicating that in an 8x8x4 core configuration the vertical interconnects are not limiting the

performance of the system and that the vertical transmission speed can be decreased to achieve higher bandwidth and increased energy efficiency. If the number of chip layers is increased, the TSVs become the bottleneck for the network performance. To show this, two simulations are run with a NoC in an 8x4x8 configuration and an 8x8x8 configuration in Figure 3-12 and Figure 3-13 respectively. The increased number of chip layers results in the expected decrease in performance.

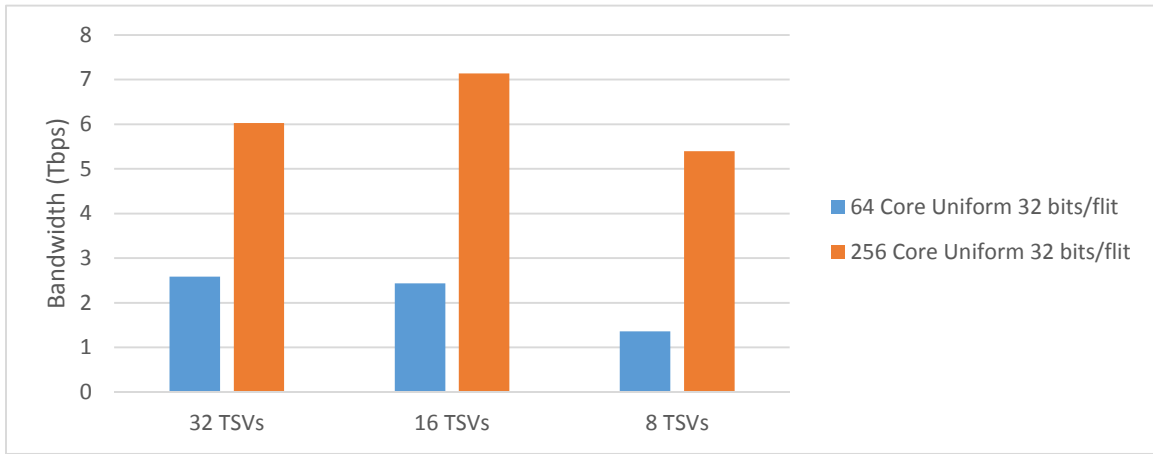


Figure 3-10: TSV Density Analysis with 32 bits/flit Uniform Traffic Peak Bandwidth

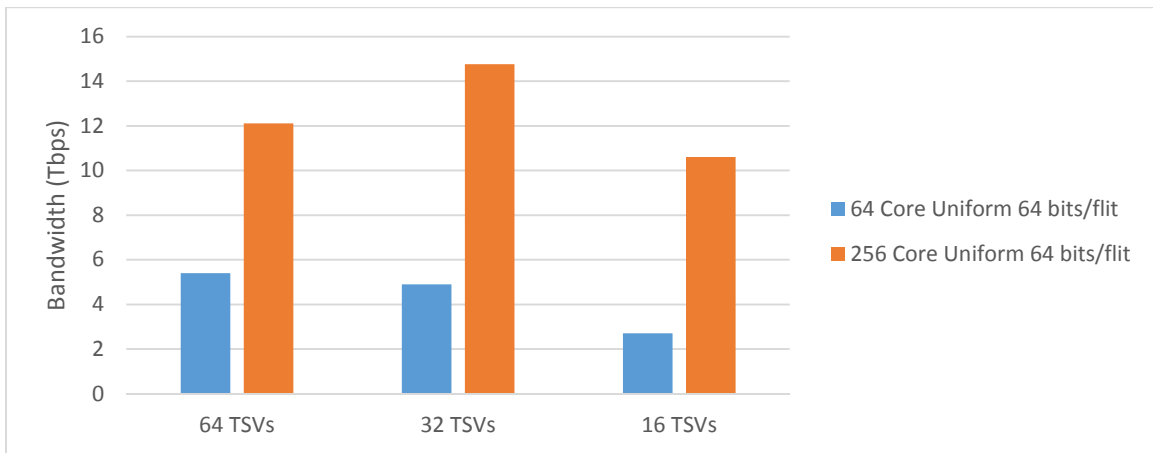


Figure 3-11: TSV Density Analysis with 64 bits/flit Uniform Traffic Peak Bandwidth

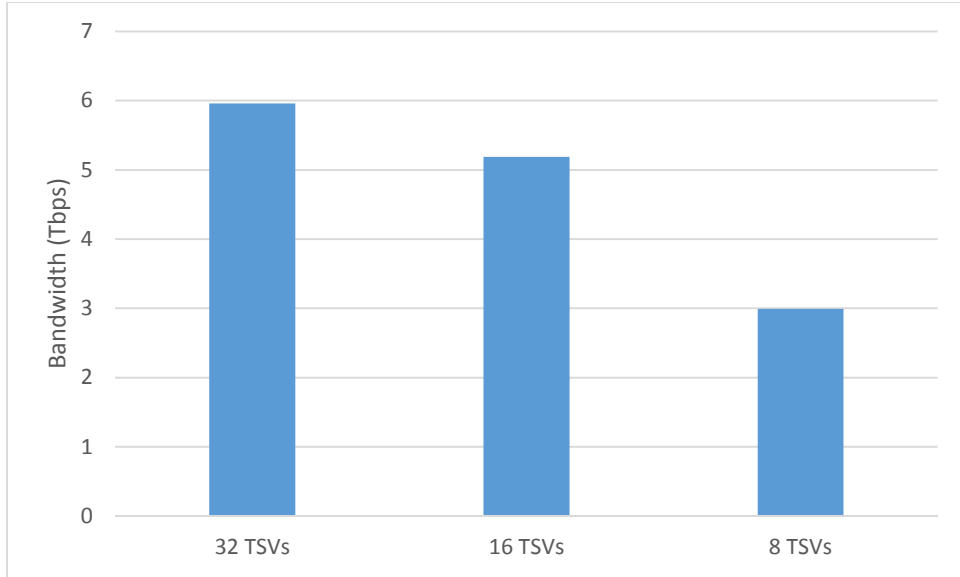


Figure 3-12: TSV Density Analysis with an 8x4x8 NoC and 32 bits/flit Uniform Traffic

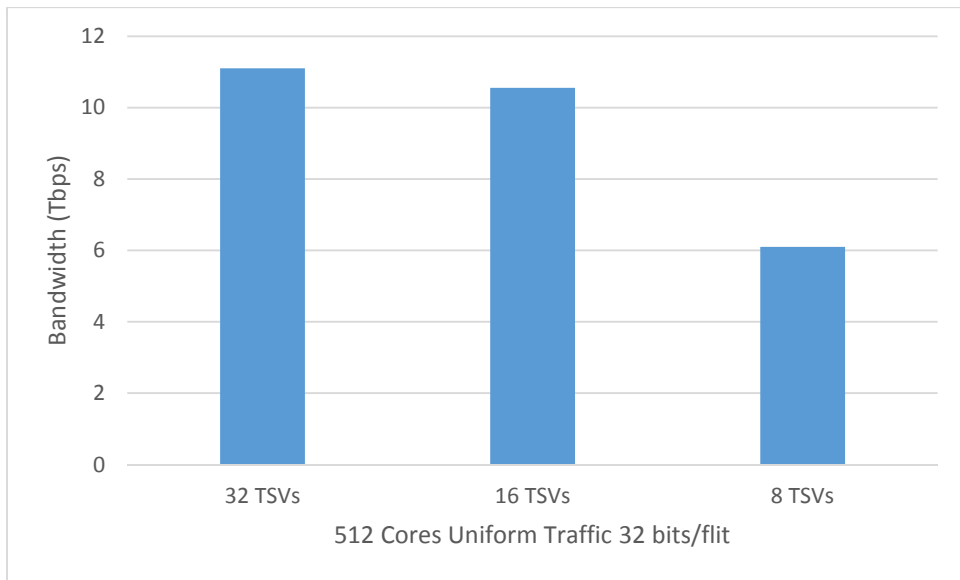


Figure 3-13: TSV Density Analysis with an 8x8x8 NoC and 32 bits/flit Uniform Traffic

### 3.5.1.2 Energy per Message

The energy per message measurements for varying the number of TSVs are shown in Figure 3-14 and Figure 3-15. In both the 32 bits per flit and the 64 bits per flit simulations, transitioning from one cycle to two cycles to transmit a flit between layers,



the 64 core systems consume slightly more energy when the network is fully loaded. This is because of the excess waiting that occurs whereas the 256 core systems have better energy efficiency when the vertical transmissions take an extra cycle. The effect quickly drops off when the vertical transmission time doubles again, however.

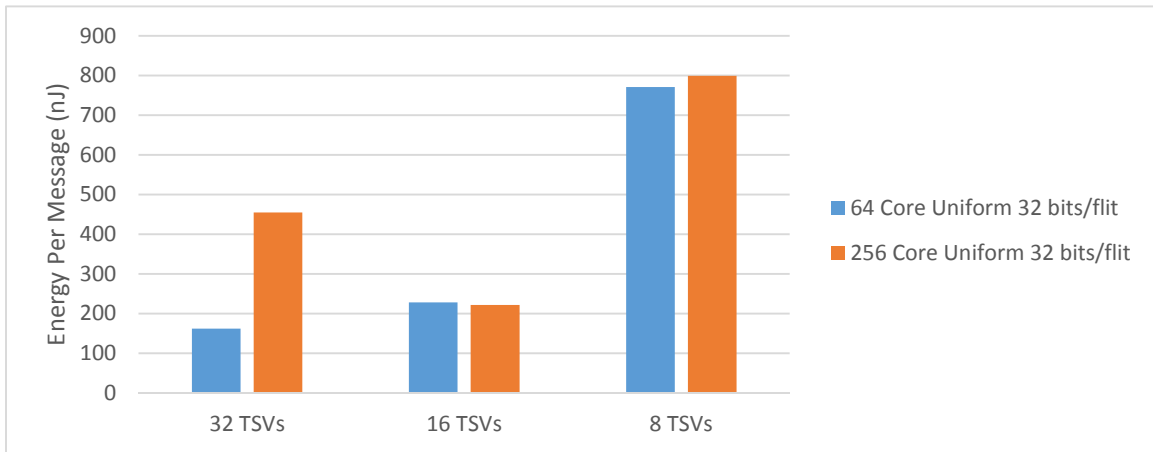


Figure 3-14: TSV Density Analysis with 32 bits/flit Uniform Traffic Energy per Message

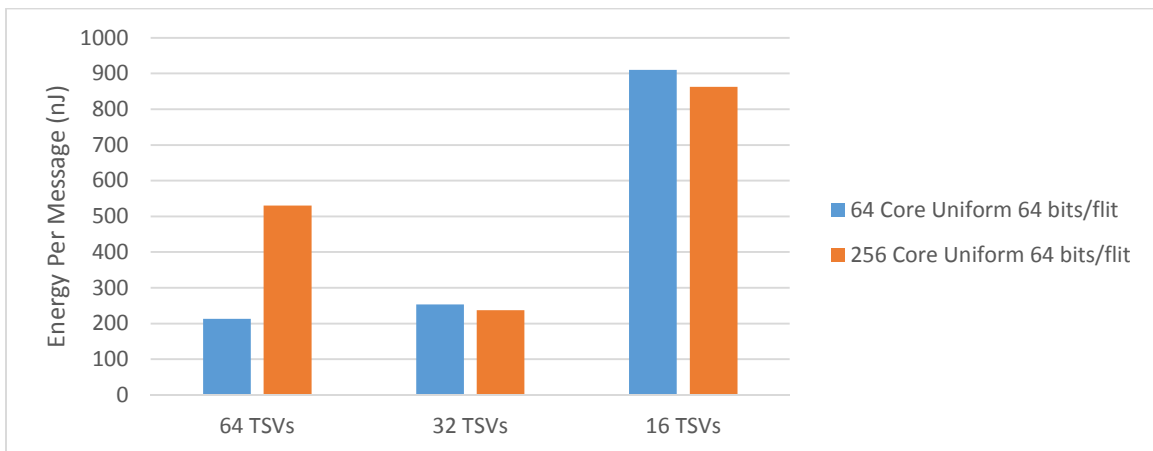


Figure 3-15: TSV Density Analysis with 64 bits/flit Uniform Traffic Energy per Message

Figure 3-16 and Figure 3-17 show the average energy dissipated per message without the waiting energy. Both the 32 bits/flit and 64 bits/flit simulations show that the data transmission energy levels off when the vertical data transfers take two cycles. The four cycle transmission time also shows a large disparity between the total energy per

message and the energy per message without the waiting component.

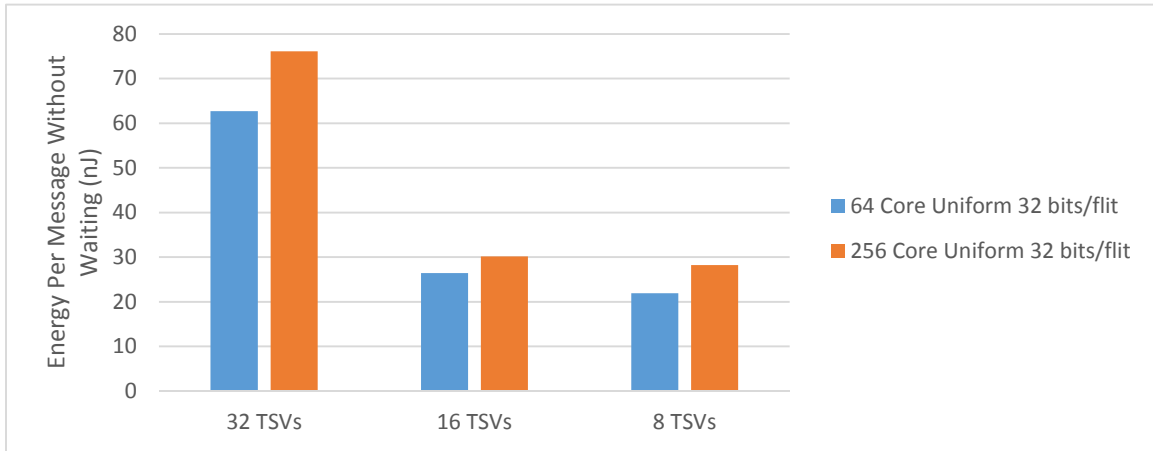


Figure 3-16: TSV Density Analysis with 32 bits/flit Uniform Traffic Energy per Message without Waiting

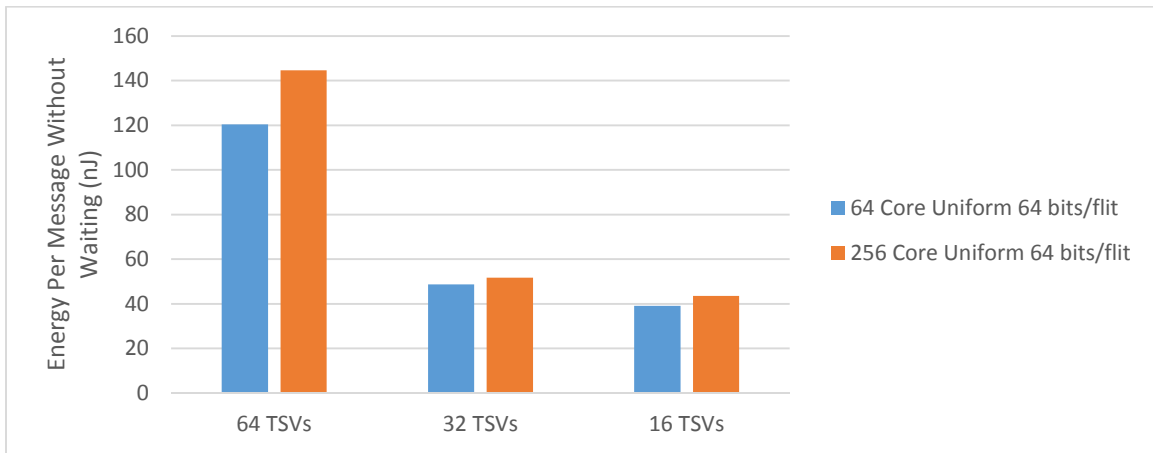


Figure 3-17: TSV Density Analysis with 64 bits/flit Uniform Traffic Energy per Message without Waiting

### 3.5.1.3 Latency

The average packet latency measurements are shown in Figure 3-18 and Figure 3-19. For 64 core systems one extra cycle for vertical transmissions in a saturated network causes the latency to increase. With 256 core systems however, the latency increase is not as noticeable. This effect also drops off when the transmission time of a flit doubles again and the latency increases significantly.

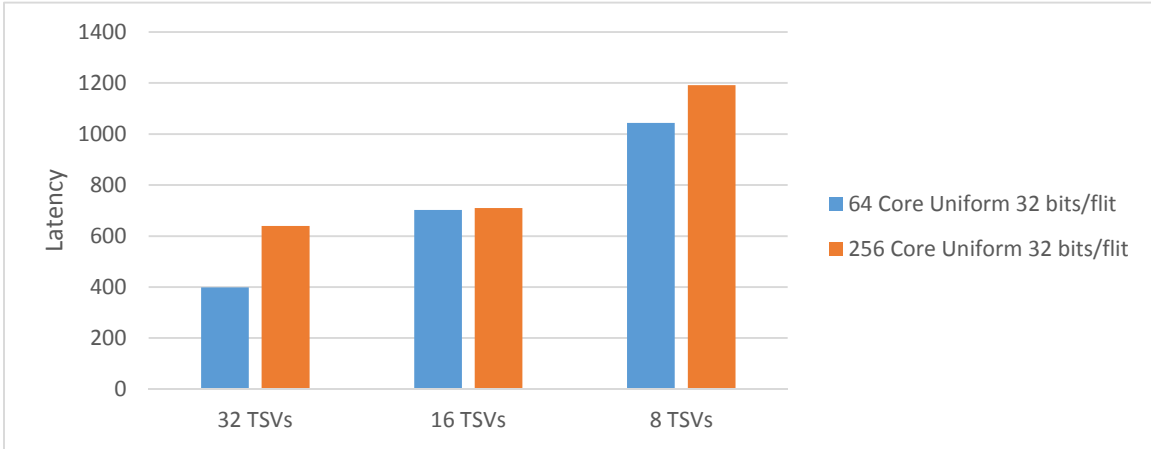


Figure 3-18: TSV Density Analysis with 32 bits/flit Uniform Traffic Average Latency

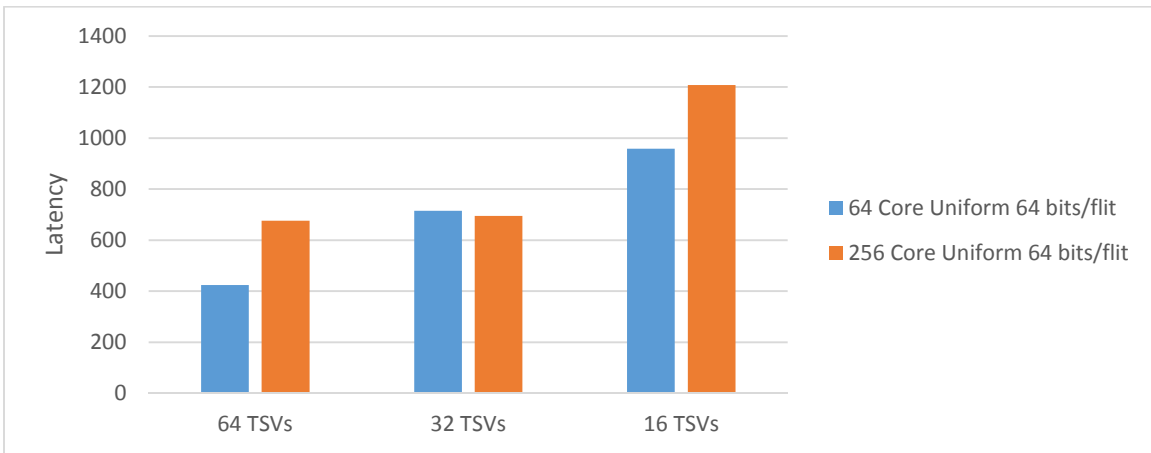


Figure 3-19: TSV Density Analysis with 64 bits/flit Uniform Traffic Average Latency

### 3.5.2 NoC Performance Evaluation with Non-Uniform Traffic

Similar to the uniform traffic simulations, the same non-uniform traffic simulations from section 3.4 are also performed with vertical data transfers taking one, two, and four cycles.

#### 3.5.2.1 Energy per Message

The energy per message for non-uniform traffic is shown in Figure 3-20 for the 32 bits/flit simulations and Figure 3-21 for the 64 bits/flit simulations. Cutting the number of

TSVs in half results in a reduction in the energy dissipation for most of the traffic patterns. A further reduction in the TSV count does not appear to reduce the energy dissipation much if at all. This is a result of the increased energy spent waiting on the network links to become free. There is a minimum point where a reduced number of TSVs allows for the minimum energy. Too few or too many TSVs and the energy increases again because the amount of energy waiting for the slower vertical links outweighs the energy savings from spreading the TSVs out.

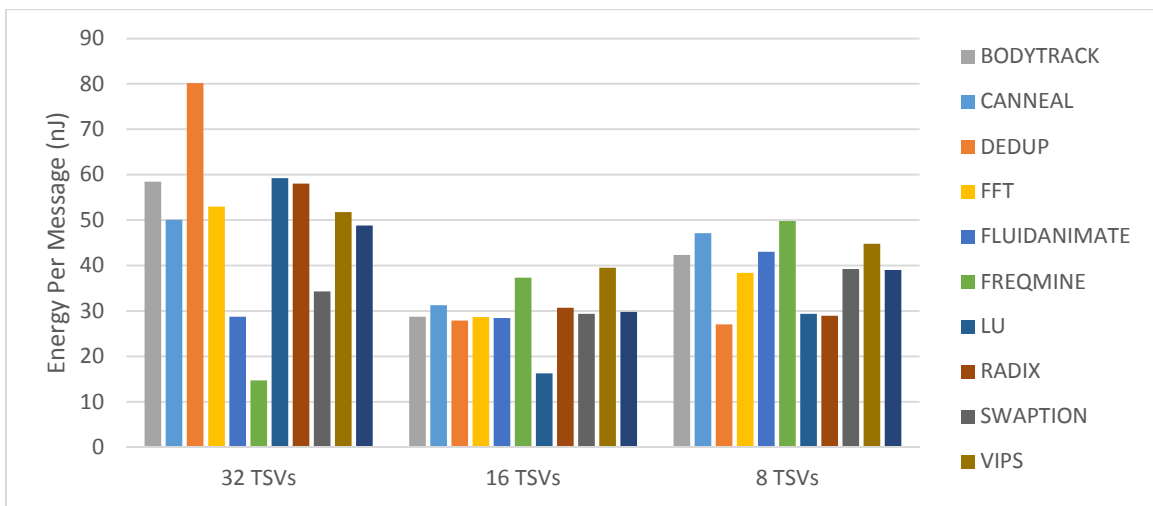


Figure 3-20: TSV Density Analysis with 32 bits/flit Non-Uniform Traffic Energy per Message

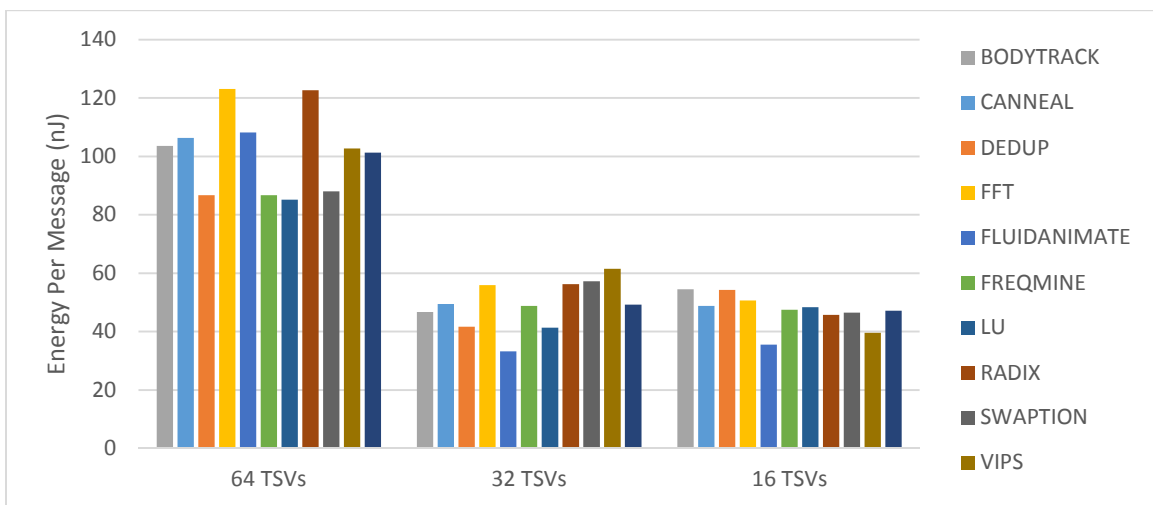


Figure 3-21: TSV Density Analysis with 64 bits/flit Non-Uniform Traffic Energy per Message

Figure 3-22 and Figure 3-23 show the average energy per message minus the energy spent waiting for the network. These graphs show a general trend of the diminishing returns that increasing the pitch between the TSVs cause. There is also a larger difference between the total energy per message and the energy per message without waiting. This is a direct result of the increased vertical transmission times.

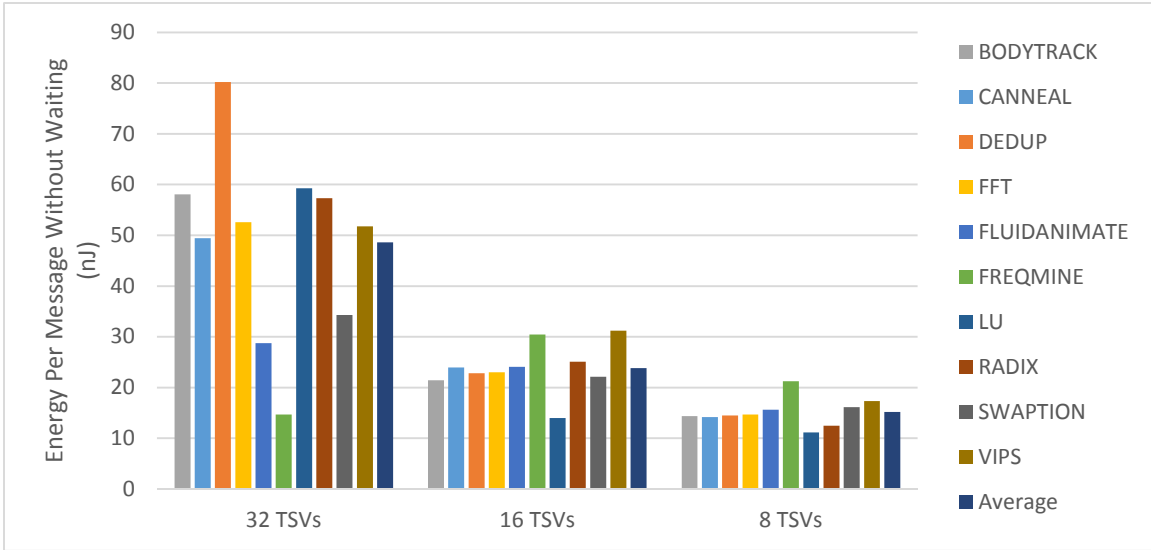


Figure 3-22: TSV Density Analysis with 32 bits/flit Non-Uniform Traffic Energy per Message without Waiting

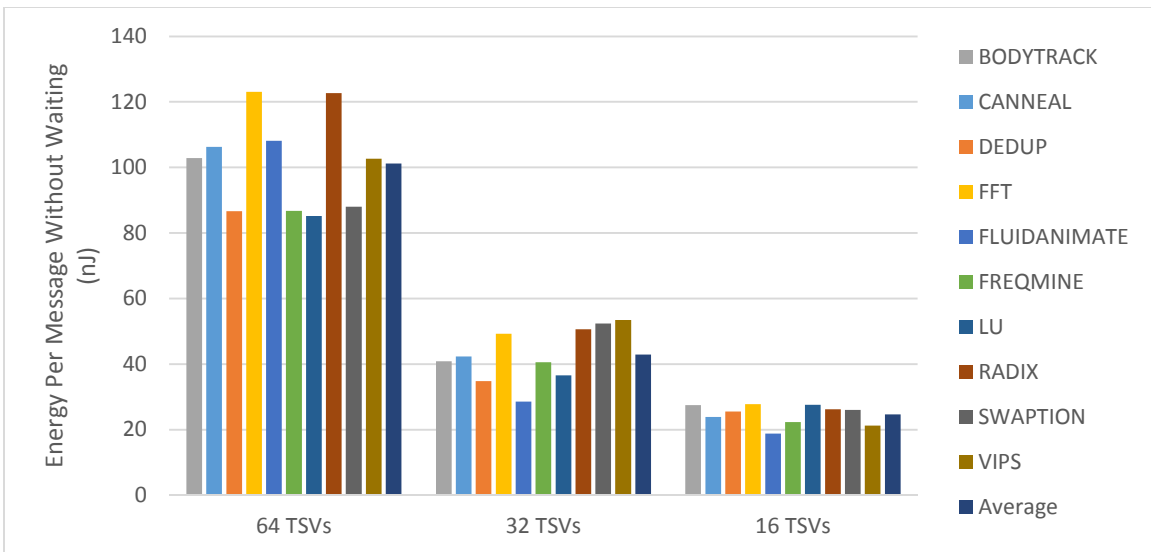


Figure 3-23: TSV Density Analysis with 64 bits/flit Non-Uniform Traffic Energy per Message without Waiting

### 3.5.2.2 Latency

The latency for non-uniform traffic is shown in Figure 3-24 and Figure 3-25. These show that the latency increases slightly when switching from one cycle to two cycles of vertical data transmission, but that it increases significantly more when going to four cycles. The increased vertical transmission times have a direct impact on the latency measurements.

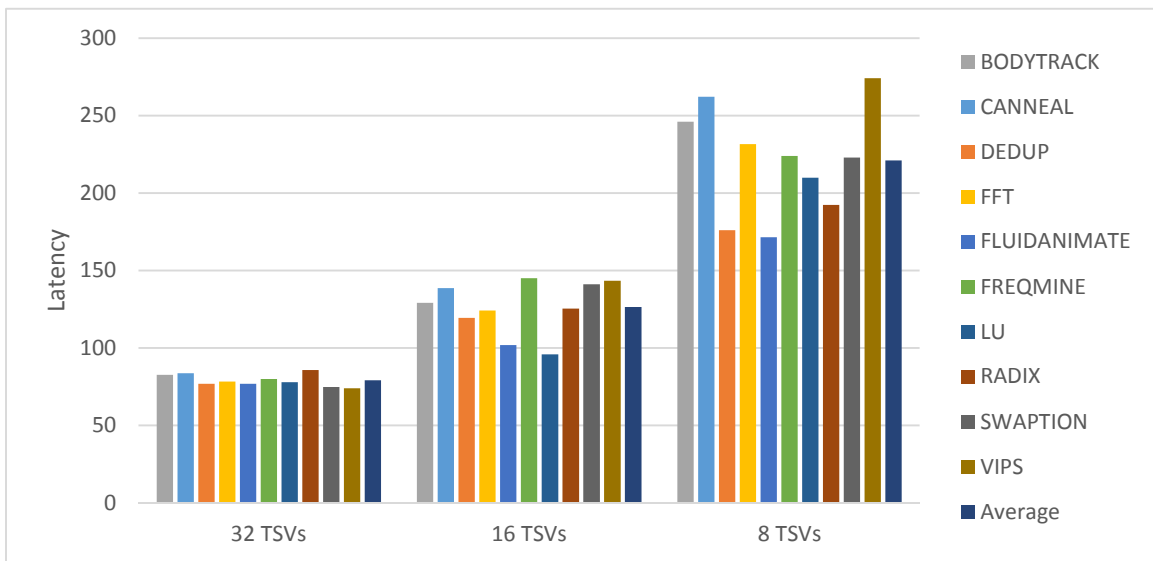


Figure 3-24: TSV Density Analysis with 32 bits/flit Non-Uniform Traffic Average Latency

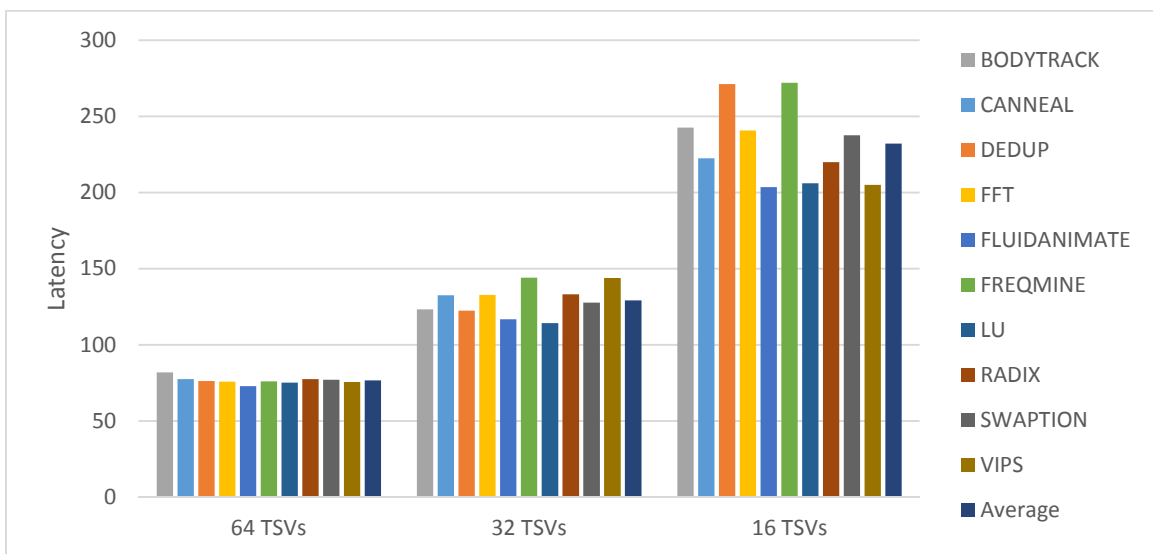


Figure 3-25: TSV Density Analysis with 64 bits/flit Non-Uniform Traffic Average Latency

### **3.6. Area Overheads**

To prevent capacitive coupling the TSVs are shielded with neighboring TSVs. This results in an overall chip area overhead for the 32 bit flit of at least  $12500\mu\text{m}^2$  using a  $5\mu\text{m}$  radius and a base pitch of  $20\mu\text{m}$  depending on the configuration. For 64 bit flits, at least  $25500\mu\text{m}^2$  are required for the TSVs. A 64 core network will need to dedicate a total of  $0.8\text{mm}^2$  for 32 bits per flit and  $1.632\text{mm}^2$  for 64 bits per flit. A 256 core network will require  $3.2\text{mm}^2$  for 32 bits per flit and  $6.528\text{mm}^2$  for 64 bits per flit. These TSVs require a relatively large chip area and are difficult to manufacture.

## Chapter 4 Wireless 3D NoC Architectures

Four network architecture and wireless vertical connection technology pairs are compared: capacitive coupling with a dense 3D mesh network, inductive coupling with a dense 3D mesh network, inductive coupling with a ring network based on [18], and inductive coupling with a proposed sparse mesh network described later in this section. The dense 3D mesh network was introduced in section 3.1 for the wired TSV networks.

Capacitive coupling requires that two chip layers be assembled in a face to face configuration. Therefore, the capacitive coupling mesh network for 64 cores is in an 8x4x2 configuration and for 256 cores is in a 16x8x2 configuration for these simulations. Other than the restriction that the number of planes is limited to two, the dense 3D mesh network is similar to the NoC described in section 3.1. Using designs mentioned in [12], the capacitive coupling links consume 15 fJ/bit and take 23 and 46 clock cycles to transfer a 32 and 64 bit flit respectively.

Inductive coupling does not have the face to face restriction and can have more than two chip layers. For the inductive coupling links, using designs from [11], energy consumption is 140 fJ/bit and it takes 3 cycles for 32 bit flits and 6 cycles for 64 bit flits. The dense 3D mesh inductive coupling networks were in 4x4x4 and 8x8x4 configurations for the 64 and 256 core systems respectively. This network architecture is also similar to the NoC described in section 3.1. The ring network originally described in [18] has vertical connections on either side of the chip as shown in Figure 4-1. The 256 core version is similar. The sparse 3D mesh network is for the 4x4x4 64 core network and has three inductive coupling links for each group of four cores on each layer to facilitate faster vertical transmission of flits. This enables single cycle vertical flit transmission



times for 32 bit flits and two cycle transmissions times for 64 bit flits. It also reduces the number of inductive coupling links required for each group of four cores by one, which saves valuable chip area. There are extra connections between cores such that any core takes at most one hop to reach a switch that has a vertical connection. The cores central to the chip contain the vertical connections. This allows for the large area of the inductive coupling circuit to be implemented so that inductive coupling pairs have minimal coupling impact on each other. One layer of the sparse 3D mesh network is shown in Figure 4-2.

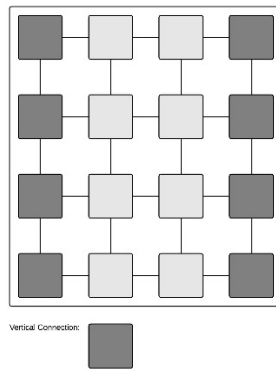


Figure 4-1: 3D Ring NoC

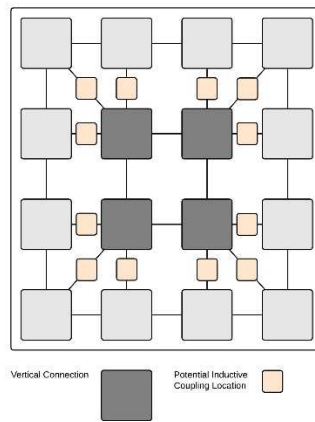


Figure 4-2: Inductive Coupling Sparse 3D Mesh NoC

## **4.1. Performance Evaluation**

The same performance metrics described in section 3.2 are utilized for the wireless 3D NoC architecture simulations. Bandwidth, energy per message, and latency measurements with uniform and non-uniform traffic for each technology and architecture pair are compared.

### **4.1.1 Bandwidth**

The peak system bandwidth for the wireless vertical connection technologies are shown in Figure 4-3 and Figure 4-4. The inductive coupling mesh networks have a higher system bandwidth than the capacitive coupling mesh network. This is mostly a result of the very high vertical communication times for the capacitive coupling architecture even though the majority of the data transfers are within the same layer. The average hop counts for the capacitive coupling networks are also higher than the other wireless networks as can be seen in Table 4-1. The inductive coupling sparse mesh lags behind the dense mesh but outperforms the ring and the capacitive coupling mesh networks. Next to the TSV vertical connections however, the wireless connections have a lower peak bandwidth. Comparing the quickest wired architectures discussed in section 3.5.1.1 and wireless architectures for the 64 core networks with 32 bits per flit the inductive coupling dense 3D mesh has a peak bandwidth 35% lower than the 32 TSV dense 3D mesh. With the 256 core networks and 32 bits per flit, the inductive coupling dense 3D mesh network is 10% slower than the 16 TSV dense 3D mesh. When analyzing the wireless 32 and 64 bits per flit simulations, the serial communication of both the inductive and capacitive coupling technologies does not scale well with increasing flit size compared to the wired TSV architectures. The bandwidth per link for 32 bits/flit is compared in Table 4-2 and

the bandwidth per link for 64 bits/flit is compared in Table 4-3. These bandwidth per link calculations help depict why the peak bandwidth varies between the technologies and architectures.

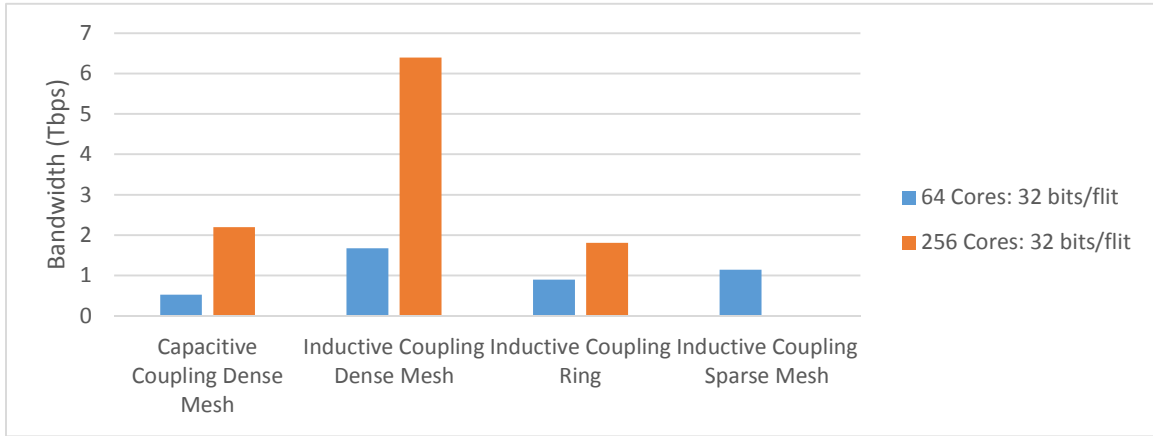


Figure 4-3: Wireless Comparison with 32 bits/flit Uniform Traffic Peak Bandwidth

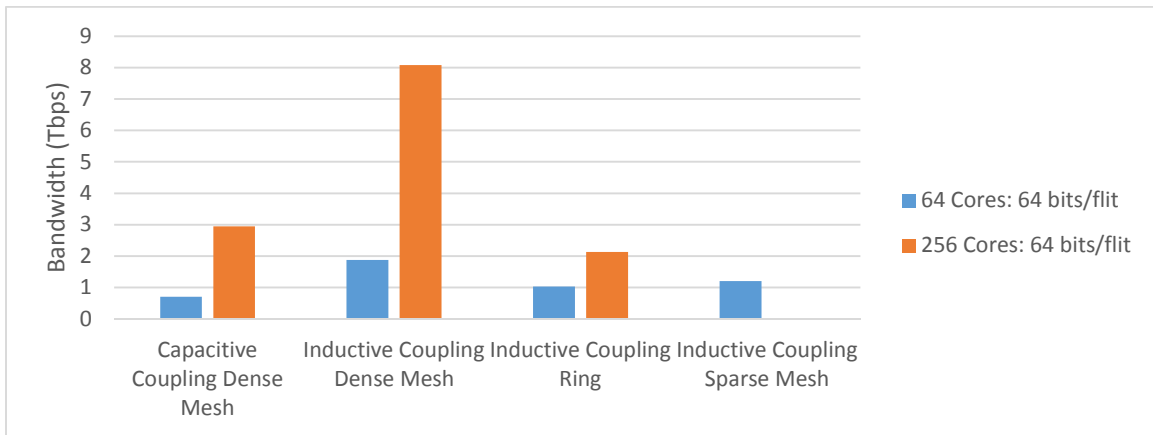


Figure 4-4: Wireless Comparison with 64 bits/flit Uniform Traffic Peak Bandwidth

Technology/Architecture Pair	Average Hop Count
64 Core Capacitive Coupling Dense 3D Mesh	4.4444
256 Core Capacitive Coupling Dense 3D Mesh	8.4706
64 Core Inductive Coupling Dense 3D Mesh	3.8095
256 Core Inductive Coupling Dense 3D Mesh	6.5255
64 Core Inductive Coupling Ring	4.1905
256 Core Inductive Coupling Ring	7.8431
64 Core Inductive Coupling Sparse 3D Mesh	3.9524

Table 4-1: Technology and Architecture Pairs System Average Hop Count Comparison

Technology/Architecture Pair	Bandwidth per Link with 32 bits/flit (Gbps)	Vertical Cycles for 32 bits/flit
32 TSV Dense 3D Mesh	80	1
16 TSV Dense 3D Mesh	40	2
8 TSV Dense 3D Mesh	20	4
Capacitive Coupling Dense 3D Mesh	3.47826087	23
Inductive Coupling Dense 3D Mesh	26.66666667	3
Inductive Coupling Ring	26.66666667	3
Inductive Coupling Sparse 3D Mesh	80	1

*Table 4-2: Technology and Architecture Pairs 32 bits/flit System Bandwidth Comparison*

Technology/Architecture Pair	Bandwidth per Link with 64 bits/flit (Gbps)	Vertical Cycles for 64 bits/flit
64 TSV Dense 3D Mesh	160	1
32 TSV Dense 3D Mesh	80	2
16 TSV Dense 3D Mesh	40	4
Capacitive Coupling Dense 3D Mesh	3.47826087	46
Inductive Coupling Dense 3D Mesh	26.66666667	6
Inductive Coupling Ring	26.66666667	6
Inductive Coupling Sparse 3D Mesh	80	2

*Table 4-3: Technology and Architecture Pairs 64 bits/flit System Bandwidth Comparison*

#### **4.1.2 Energy per Message**

The energy per message for the wireless connection architectures are compared in Figure 4-5 and Figure 4-6. The capacitive coupling network consumes a considerable amount of energy compared to the other network architecture and technology pairs except for the inductive coupling ring with 256 cores. As Table 4-2 and Table 4-3 show, each capacitive coupling link takes several more clock cycles than any of the other architecture technology pairs causing the network to become congested. The inductive coupling ring with 256 cores spends a considerable amount of time waiting on network congestion as a result of the ring architecture. Highly congested networks spend more time and energy waiting for the links to become free than networks that have more free links. The sparse

mesh network consumes less energy than the ring network but is less efficient than the inductive coupling dense mesh network. For the sparse mesh network, three times as much energy is dissipated in a single cycle for the vertical transmissions compared to the other inductive coupling networks. It makes up for the increased energy consumption in one cycle by decreasing the overall latency. In a fully loaded network, the four switches in a layer that handle the vertical transmissions are traffic hotspots that bottleneck the system and dissipate extra energy compared to the dense mesh network. For each of the networks other than the ring architecture, the energy per message for 256 core networks does not change much from the 64 core networks because the number of vertical transmissions per message are similar. The 256 core ring network, however, spends a lot of time waiting for the vertical links to be free. When comparing flit sizes of 32 and 64 bits for each architecture, the energy per message approximately doubles due to the limitations of the wireless serial communications and their poor scaling.

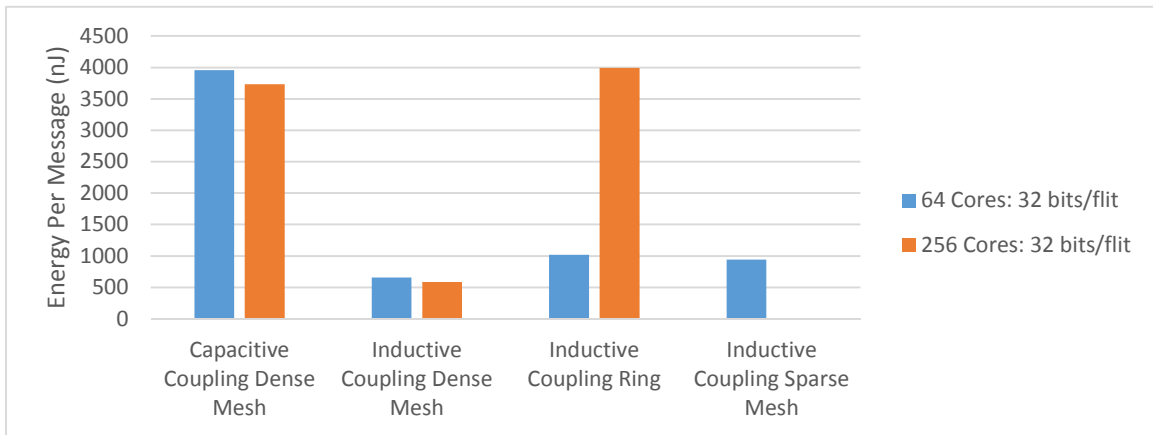


Figure 4-5: Wireless Comparison with 32 bits/flit Uniform Traffic Energy per Message

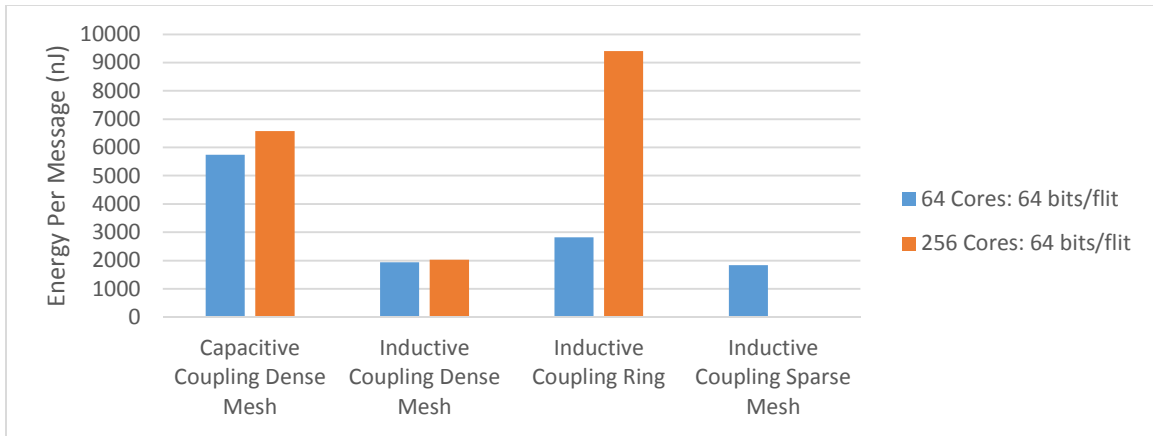


Figure 4-6: Wireless Comparison with 64 bits/flit Uniform Traffic Energy per Message

Figure 4-7 and Figure 4-8 show the energy consumption of just the data transmission. Most of the wireless architecture and technology pairs dissipate the majority of their energy per message waiting for the network. The capacitive coupling mesh network has a higher energy dissipation because of the slow link speeds. The 64 core inductive coupling ring network spends about 20% of the energy on data because of the high network congestion. The 256 core ring network is even worse with 9%. The inductive coupling dense mesh dissipates about 30% of the energy per message in the data transmissions. The sparse mesh inductive coupling network on the other hand spends more energy on transferring data than the other architecture and technology combinations. It dissipates about 50% of the total energy per message in the data transmissions and is the most efficient from a wasted energy point of view. The efficiencies for networks using 64 bits per flit are worse than networks using 32 bits per flit again because of the increased network congestion and poor scaling.

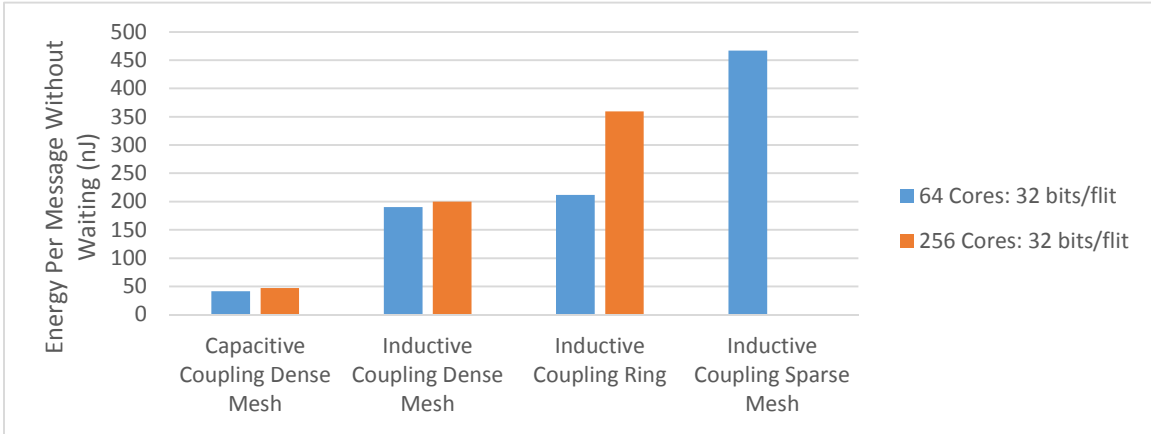


Figure 4-7: Wireless Comparison with 32 bits/flit Uniform Traffic Energy per Message without Waiting

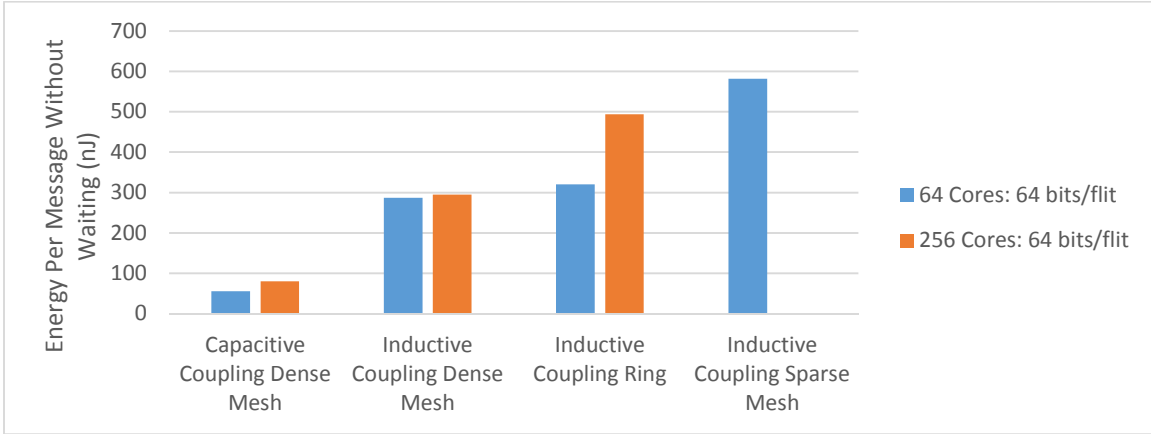


Figure 4-8: Wireless Comparison with 64 bits/flit Uniform Traffic Energy per Message without Waiting

### 4.1.3 Latency

The latency from header flit insertion to tail flit absorption is shown in Figure 4-9 and Figure 4-10. The sparse mesh network has a lower latency than the other inductive coupling networks. The single cycle vertical transmission time compared to the longer transmission times of the other architectures as described in Table 4-2, enables the sparse mesh architecture to maintain lower latencies. It has slightly less of an advantage compared to the capacitive coupling mesh network because the majority of the capacitive coupling communications occur within the same chip layer even though the capacitive

links take several more cycles to transmit each individual flit between chip layers. The inductive coupling sparse 3D mesh actually has a higher latency than the capacitive coupling dense mesh when using 64 bits per flit. In practice the network is usually not as saturated as it is with uniform traffic. Non-uniform traffic patterns give a better representation of a real application's communication latency and is explored in more detail for the wireless architectures in section 4.2.2.

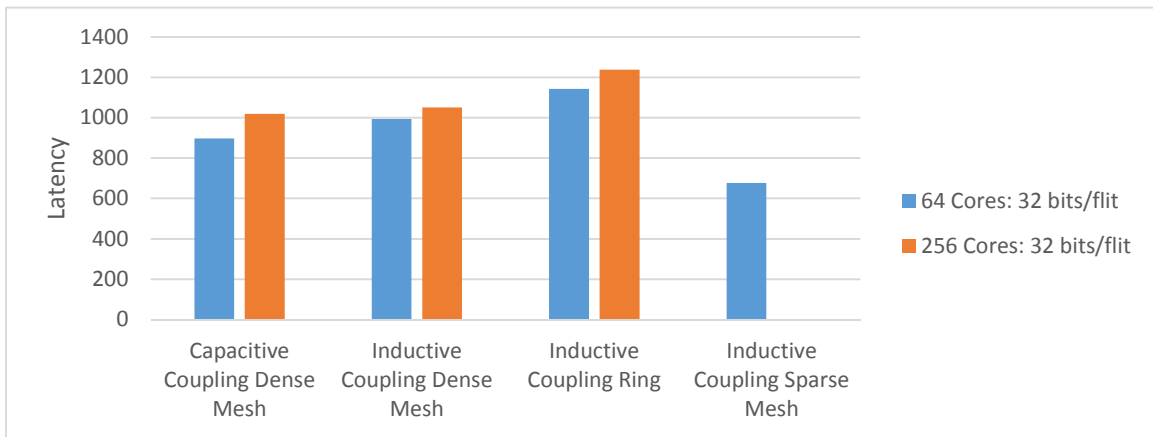


Figure 4-9: Wireless Comparison with 32 bits/flit Uniform Traffic Average Latency

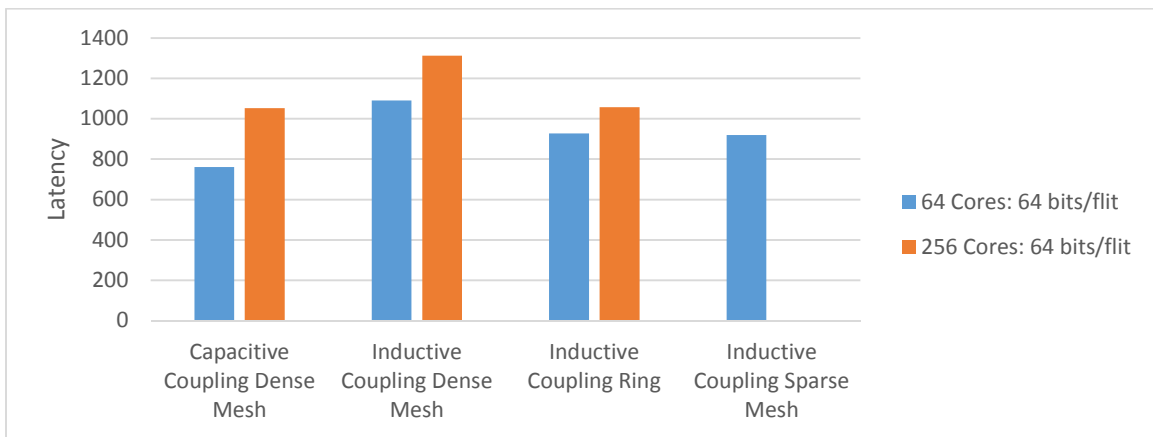


Figure 4-10: Wireless Comparison with 64 bits/flit Uniform Traffic Average Latency

## 4.2. Performance Evaluation with Non-Uniform Traffic

Similar to section 3.4, the NoCs are also compared with common non-uniform traffic patterns. Analysis of the energy per message and latency is done for all of the



wireless architectures with the benchmarks BODYTRACK, CANNEAL, DEDUP, FFT, FLUIDANIMATE, FREQMINE, LU, RADIX, SWAPTION, and VIPS.

### 4.2.1 Energy per Message

The energy per message for non-uniform traffic is compared in Figure 4-11 and Figure 4-12. Similar to the uniform traffic results in section 4.1.2, the sparse mesh network in practice consumes considerably more energy than the other networks. The capacitive coupling simulations vary widely depending on which traffic patterns tried to send data over the vertical connections, but overall consumed more energy than the inductive coupling dense mesh and ring networks. For traffic patterns utilizing 64 bits per flit, the capacitive coupling network consumes more energy per message than even the sparse 3D mesh. As depicted in Table 4-2 and Table 4-3, the high vertical transmission time contributes to a congested network for traffics that send data from one end of the chip to the other. The inductive coupling ring and mesh networks had similar energy dissipation. The energy saving benefits of having fewer inductive coupling links in the ring network is balanced by the reduced waiting time of the dense 3D mesh.

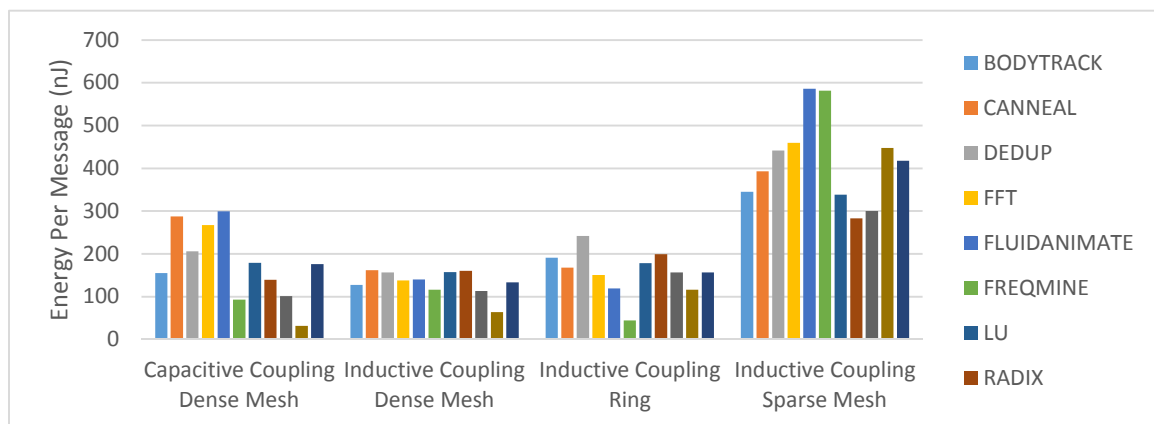


Figure 4-11: Wireless Comparison with 32 bits/flit Non-Uniform Traffic Energy per Message

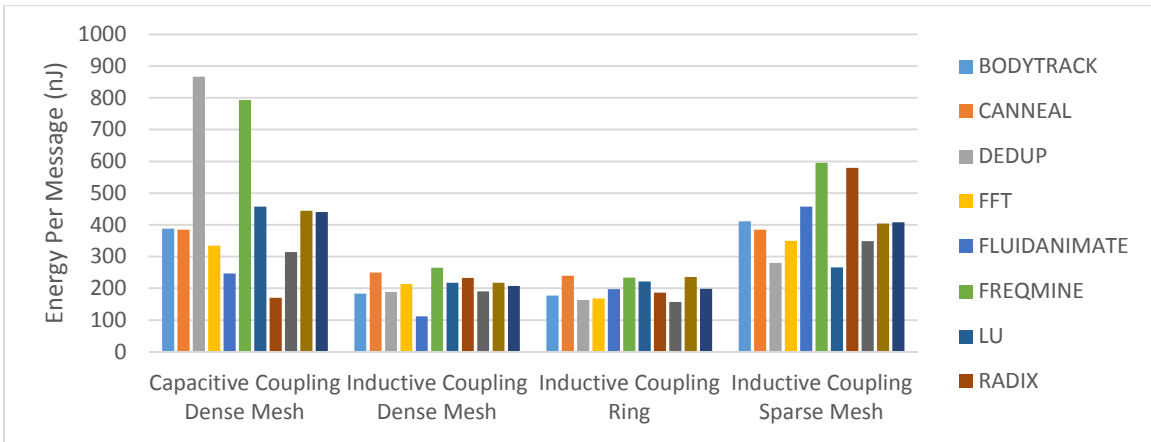


Figure 4-12: Wireless Comparison with 64 bits/flit Non-Uniform Traffic Energy per Message

Figure 4-13 and Figure 4-14 show the energy dissipation without waiting. The capacitive coupling network energy dissipation is mostly from waiting on the vertical connections because of the extended vertical transmission times and high network congestion. The inductive coupling networks rarely required any waiting so the energy dissipation without waiting is close to the overall energy dissipation. The ring network has the greatest energy dissipation disparity, with the dense 3D mesh closely following. The sparse 3D mesh has the least disparity between the two measurements and spends most of the overall energy transferring data between each of the cores.

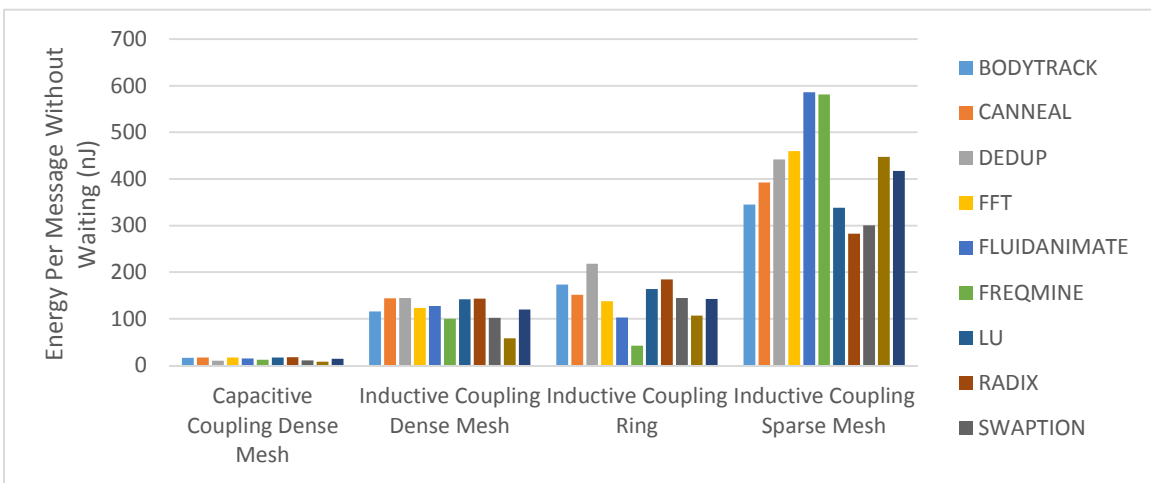


Figure 4-13: Wireless Comparison with 32 bits/flit Non-Uniform Traffic Energy per Message without Waiting

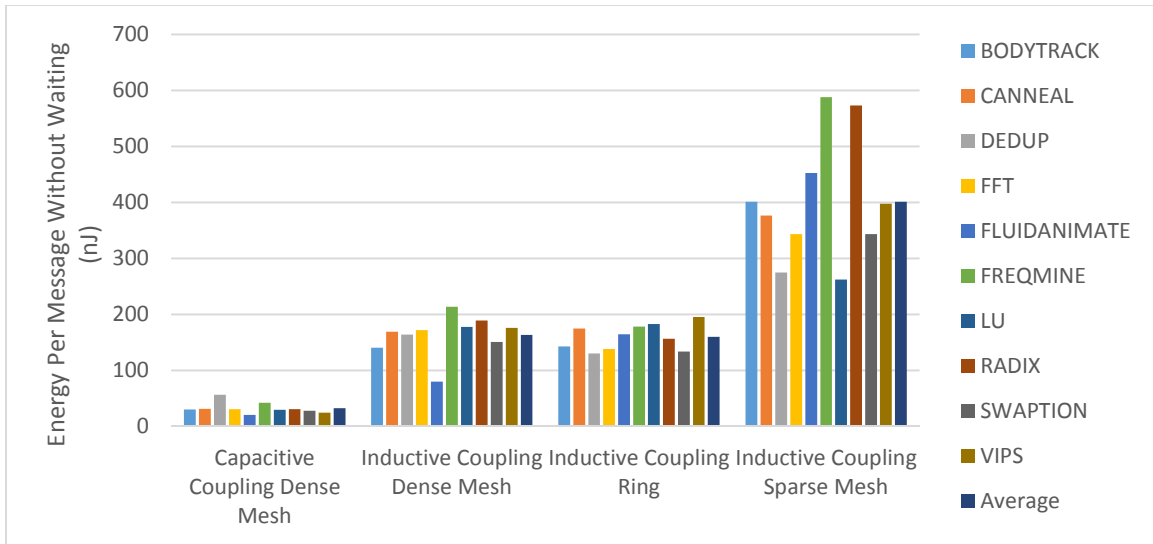


Figure 4-14: Wireless Comparison with 64 bits/flit Non-Uniform Traffic Energy per Message without Waiting

## 4.2.2 Latency

The average latency for the non-uniform traffic patterns are shown in Figure 4-15 and Figure 4-16. The inductive coupling sparse mesh does really well performance wise and is only slightly behind the quickest TSV results while outperforming the slower TSV networks that use 32 bits per flit and staying competitive with the slower TSV networks that use 64 bits per flit. The energy increase for typical workloads may not be worth the performance increase compared to the other inductive coupling networks. For instances where a wireless interconnect is essential, such as the implementation of a liquid cooling layer, the sparse 3D mesh could be the best option to maintain similar vertical performance to the rest of the chip using TSVs. The capacitive coupling mesh does not perform as well. It consumes a lot of extra energy and the latency is significantly higher compared to all of the inductive coupling networks. The high vertical transmission time as illustrated by Table 4-2 and Table 4-3 is the main contributor to the excess latency compared to the other networks. On average, the inductive coupling ring network is only

slightly slower than the full 3D mesh. The network congestion at the inductive coupling links and the higher average hop count plays a role in the increased latency.

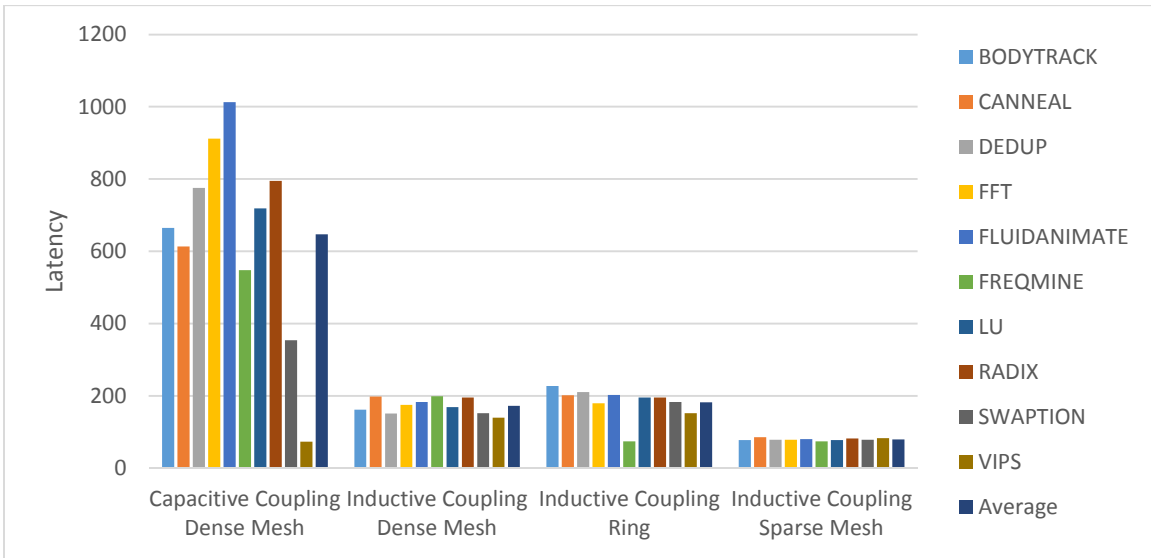


Figure 4-15: Wireless Comparison with 32 bits/flit Non-Uniform Traffic Average Latency

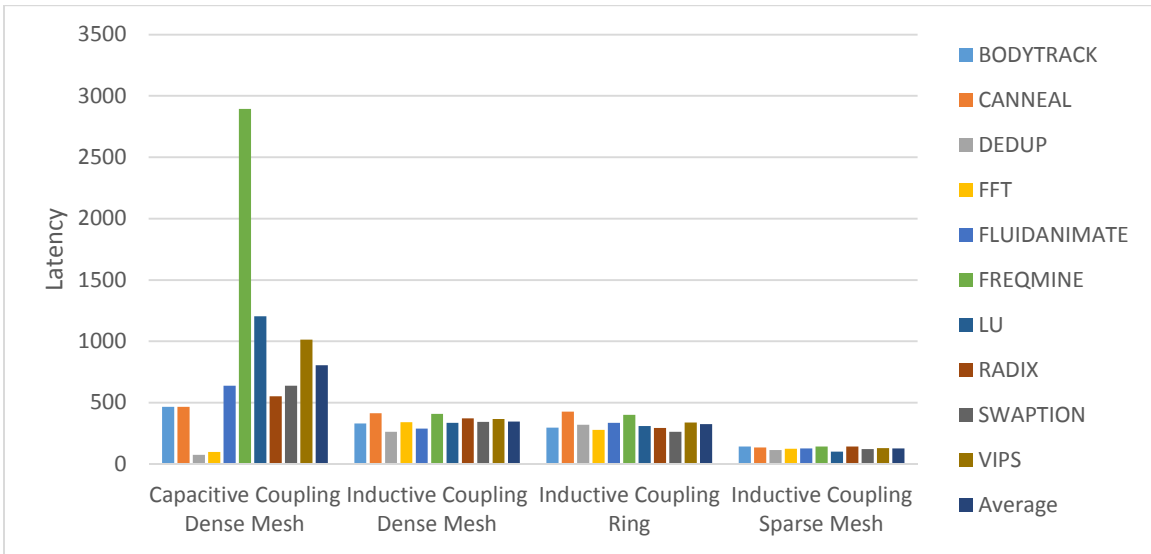


Figure 4-16: Wireless Comparison with 64 bits/flit Non-Uniform Traffic Average Latency

### 4.3. Area Overheads

According to [11] and [12], each capacitive coupling transceiver would require at least  $320\mu\text{m}^2$  and each inductive coupling transceiver would need at least  $900\mu\text{m}^2$ . As demonstrated in Table 4-4, the area needed for the wireless interconnects is significantly

smaller than the required area for TSVs. These wireless technologies also do not require any additional manufacturing steps, unlike TSVs.

Technology/Architecture Pair	Per Link Chip Area (um <sup>2</sup> )	64 Core Total Chip Area (um <sup>2</sup> )	256 Core Total Chip Area (um <sup>2</sup> )
TSV Dense 3D Mesh 32 bits/flit	12500	800000	3200000
TSV Dense 3D Mesh 64 bits/flit	25500	1632000	6528000
Capacitive Coupling Dense 3D Mesh	320	20480	81920
Inductive Coupling Dense 3D Mesh	900	57600	230400
Inductive Coupling Ring	900	28800	57600
Inductive Coupling Sparse 3D Mesh	900	14400	N/A

*Table 4-4: Technology and Architecture Pairs System Chip Area Overhead Comparison*

## **Chapter 5 Conclusions**

### **5.1. Summary**

The TSV 3D mesh has the highest bandwidth, lowest energy consumption, and lowest latency of all of the network architectures. Of the wireless architectures, the inductive coupling dense 3D mesh had the highest bandwidth and lowest energy, but the inductive coupling sparse 3D mesh maintained a much lower latency. If wireless interconnects are not required and manufacturing permits, a TSV 3D mesh would be ideal. When choosing between wireless architectures, inductive coupling is better than capacitive coupling but which architecture to use will depend on the design constraints. An energy constrained system would benefit more from a dense 3D mesh while a latency constrained system would benefit more from a sparse 3D mesh.

#### **5.1.1 System Bandwidth**

In a system bandwidth comparison, the wired TSV mesh outperforms all of the wireless architectures by at least 54.874% for 64 cores and 32 bits per flit. It also outpaces the wireless architectures by at least 187.296% for 64 cores and 64 bits per flit because of the relatively low bits per flit scalability of the wireless architectures. For 256 cores and 32 bits per flit, the wired TSV mesh is 11.613% faster than the wireless architectures only if the number of TSVs is cut in half so that vertical transmissions of flits take two clock cycles. Similarly, for 256 cores and 64 bits per flit, the 32 TSV wired mesh is 82.662% faster than the wireless architectures. The number of chip layers also affects the overall chip performance when analyzing the TSV density. The single cycle

vertical transmission time and high vertical connectivity contribute to the TSVs high bandwidth performance.

When analyzing just the wireless architectures, the inductive coupling dense 3D mesh is 46.598% faster than the inductive coupling sparse 3D mesh, 85.565% faster than the inductive coupling ring, and 220.428% faster than the capacitive coupling mesh network with 64 cores and 32 bits per flit. With 256 cores and 32 bits per flit, the inductive coupling dense 3D mesh is 191.502% faster than the capacitive coupling network and 253.52% faster than the inductive coupling ring network. Similarly with 64 cores and 64 bits per flit, the inductive coupling dense 3D mesh is 55.499% faster than the inductive coupling sparse 3D mesh, 82.012% faster than the inductive coupling ring, and 167.346% faster than the capacitive coupling 3D mesh. With 256 cores and 64 bits per flit, the inductive coupling dense 3D mesh is 173.901% faster than the capacitive coupling network and 278.162% faster than the inductive coupling ring. With 64 and 256 cores, the lower vertical transmission times and high vertical connectivity help the inductive coupling dense 3D mesh maintain the highest bandwidth. With 256 cores, the longer vertical transmission times for the capacitive coupling network is balanced with the increased percentage of same layer packet transmissions that lead to higher bandwidths than the inductive coupling ring.

### **5.1.2 System Energy per Message**

Analyzing the energy per message for uniform traffic patterns with 32 bits per flit and 64 cores, the TSV mesh has a 75.359% reduction in energy consumption compared to the inductive coupling dense 3D mesh. With 64 bits per flit and 64 cores, the TSV mesh has an 88.397% reduction in energy consumption compared to the inductive

coupling sparse 3D mesh. Similarly, the 32 TSV 256 core system with 32 bits per flit shows a 62.1% reduction in energy from the inductive coupling dense 3D mesh. The 32 TSV 256 core system with 64 bits per flit has an 88.321% decrease in energy compared to the inductive coupling dense 3D mesh. As a technology, the TSVs are better at scaling both the number of bits per flit and the number of cores in the system than the wireless architectures.

In a pure wireless architecture comparison with 64 cores and 32 bits per flit, the inductive coupling dense 3D mesh uses 30.183% less energy than the inductive coupling sparse 3D mesh, 35.541% less energy than the inductive coupling ring, and 83.367% less than the capacitive coupling network. With 64 bits per flit, the inductive coupling sparse 3D mesh uses 5.296% less energy than the inductive coupling dense mesh, has a 34.921% reduction compared to the inductive coupling ring, and 68.049% less than the capacitive coupling mesh. Looking at 256 core wireless systems with 32 bits per flit, the inductive coupling dense 3D mesh has an 84.303% decrease in energy per message compared to the capacitive coupling mesh and an 85.324% reduction compared to the inductive coupling ring network. For 256 cores and 64 bits per flit, the inductive coupling dense 3D mesh uses 69.11% less energy than the capacitive coupling 3D mesh and 78.391% less energy than the inductive coupling ring. In general, the inductive coupling dense 3D mesh uses less energy than the other networks except for 64 cores and 64 bits per flit at which point the inductive coupling sparse mesh has a slight edge. The two cycle transmission times help the network use less energy than the six cycle transmission times for the inductive coupling dense 3D mesh network. Both of the inductive coupling mesh networks have fairly high vertical connectivity which helps them balance the high



network congestion in the uniform traffic. The sparse mesh utilizes faster vertical links that help save energy at full network loads compared to the dense mesh with 64 bits per flit. When scaled to 256 cores, the capacitive coupling mesh has a higher percentage of same plane communications which use much less energy than vertical transmissions. This allows it to be more energy efficient than the inductive coupling ring but not nearly as efficient as the inductive coupling dense 3D mesh and its high vertical connectivity and lower vertical latency.

With non-uniform traffic patterns utilizing 64 cores and 32 bits per flit, the 16 TSV dense 3D mesh uses 77.672% less energy than the inductive coupling dense 3D mesh, 80.94% less than the inductive coupling ring, 83.048% less than the capacitive coupling mesh, and 92.854% less than the inductive coupling sparse mesh. Similarly, with 64 bits per flit, the 16 TSV dense 3D mesh has a 76.204% decrease in energy usage from the inductive coupling ring network, a 77.252% decrease from the inductive coupling dense 3D mesh, an 88.443% decrease from the inductive coupling sparse 3D mesh, and an 89.292% reduction in energy from the capacitive coupling mesh network. The TSVs use considerably less energy than any of the wireless architectures and also scale well with increasing flit size. The energy per bit for transmitting data across a TSV is significantly lower than the wireless architectures. Also, when analyzing the effect that the TSV density has on energy consumption with non-uniform traffic patterns, there is a minimum energy point. Too many or too few TSVs will increase the energy consumption because the amount of energy spent waiting for the slower network links will outweigh the energy savings from spreading the TSVs apart.

Among the wireless networks with 32 bits per flit, the inductive coupling dense 3D mesh uses 14.635% less energy than the inductive coupling ring network, 24.077% less than the capacitive coupling mesh, and 67.996% less than the inductive coupling sparse 3D mesh. The 64 bits per flit simulations reveal that the inductive coupling ring network has an energy reduction of 4.405% compared to the inductive coupling dense 3D mesh, 51.435% compared to the inductive coupling sparse 3D mesh, and 54.999% compared to the capacitive coupling mesh network. For most non-uniform traffic patterns, the inductive coupling ring network shows good energy scaling with the number of bits per flit. The capacitive coupling mesh utilized more energy than the other networks because of its high vertical transmission latency and high energy per bit for transmitting across a capacitive coupling link despite that a higher percentage of messages being transmitted were in the same layer. The inductive coupling sparse mesh sacrifices energy efficiency for lower network latency which causes its energy measurements to suffer with low bandwidth non-uniform traffic patterns. The inductive coupling dense 3D mesh energy usage scales relatively well with the number of bits per flit compared to the other wireless networks.

### **5.1.3 System Latency**

Analyzing the latency metrics gathered from the uniform traffic 64 core and 32 bits per flit simulations, the 32 TSV dense 3D mesh has an average latency 41.094% less than the inductive coupling sparse 3D mesh, 55.599% less than the capacitive coupling dense 3D mesh, 59.871% less than the inductive coupling dense 3D mesh, and 65.112% less than the inductive coupling ring network. With 64 bits per flit, the messages for the 64 TSV dense 3D mesh take 44.221% fewer cycles than the capacitive coupling mesh,

53.885% fewer clock cycles than the inductive coupling sparse 3D mesh, 54.273% less time than the inductive coupling ring network, and 61.102% less time than the inductive coupling dense 3D mesh. Increasing the number of cores to 256 with 32 bits per flit, the 32 TSV dense 3D mesh has an average latency 37.206% less than the capacitive coupling mesh, 39.081% lower than the inductive coupling dense 3D mesh, and 46.271% less than the inductive coupling ring network. With 64 bits per flit, the 64 TSV mesh takes 35.848% fewer cycles to transmit a message than the capacitive coupling mesh, 36.128% less time than the inductive coupling ring, and 48.556% less than the inductive coupling dense 3D mesh network. The high vertical connectivity and single cycle latency of the TSV dense 3D mesh network results in the quickest message transmissions for each of the uniform traffic simulations.

When comparing the 64 core and 32 bits per flit wireless architecture latencies, the inductive coupling sparse 3D mesh takes 24.623% less time for message transfers than the capacitive coupling network, 31.875% less than the inductive coupling dense 3D mesh, and 40.773% less than the inductive coupling ring network. With 64 bits per flit, the capacitive coupling mesh message transfers take 17.325% fewer cycles than the inductive coupling sparse 3D mesh, 18.021% fewer than the inductive coupling ring network, and 30.264% less than the inductive coupling dense 3D mesh. Moving to 256 cores and 32 bits per flit, the capacitive coupling mesh messages use 2.986% fewer cycles for message transfers than the inductive coupling dense 3D mesh and 17.69% less than the inductive coupling ring. With 64 bits per flit, the capacitive coupling mesh take 0.437% less time than the inductive coupling ring and 19.809% less than the inductive coupling dense 3D mesh. The capacitive coupling mesh has a lower latency mostly

because a high percentage of the messages being transmitted do not need to go across a capacitive link. The single cycle transmit times for the inductive coupling sparse 3D mesh help it stay competitive with the other networks. The inductive coupling ring network has a slightly lower latency than the inductive coupling dense 3D mesh when there are 64 bits per flit because a higher percentage of the packet routing is in the same layer and the network is so congested that packets will wait long periods of time for a vertical link to become free.

For non-uniform traffic patterns with 64 cores and 32 bits per flit, the 32 TSV mesh has only a 0.244% cycle time decrease compared to the inductive coupling sparse 3D mesh, a 54.04% decrease compared to the inductive coupling dense 3D mesh, a 56.476% decrease from the inductive coupling ring network latency, and an 87.76% decrease compared to the capacitive coupling mesh. With 64 bits per flit, the 64 TSV mesh message transfers take 40.37% less time than the inductive coupling sparse 3D mesh, 76.595% less time than the inductive coupling ring, 77.938% less than the inductive coupling dense 3D mesh, and 90.495% less than the capacitive coupling mesh. Again, the high vertical connectivity and single cycle latency help to keep the TSVs outperforming the other network architectures in terms of message latency.

A comparison of the wireless architectures by themselves with non-uniform traffic, 64 cores, and 32 bits per flit shows that the inductive coupling sparse 3D mesh latency is 53.928% lower than the inductive coupling dense 3D mesh, 56.37% lower than the inductive coupling ring, and 87.73% lower than the capacitive coupling network. With 64 bits per flit, the inductive coupling sparse 3D mesh latency is 60.749% lower than the inductive coupling ring, 63.002% lower than the inductive coupling dense 3D

mesh, and 84.059% lower than the capacitive coupling mesh. With practical network loads, the inductive coupling sparse 3D mesh is able to utilize its extra planar links and vertical bandwidth to reduce the latencies to a minimum.

#### **5.1.4 Chip Area**

The chip area overheads for the various architectures for 64 cores from most demanding space requirements to the least space needed for implementation is the TSV dense 3D mesh with 64 bits per flit, the TSV dense 3D mesh with 32 bits per flit, the inductive coupling dense 3D mesh, the inductive coupling ring, the capacitive coupling dense 3D mesh, and finally, the inductive coupling sparse 3D mesh. For 256 cores, the TSV dense 3D mesh with 64 bits per flit is still requires the most space followed by the TSV dense 3D mesh with 32 bits per flit. Then comes the inductive coupling dense 3D mesh, the capacitive coupling dense 3D mesh, and lastly, the inductive coupling ring. The TSV networks require a large amount of space because each TSV needs to be separated by a ground or power TSV to prevent capacitive coupling. Encoding schemes could remove the need for extra TSVs but the added complexity may outweigh the benefits. The inductive coupling sparse 3D mesh has fewer vertical links than the inductive coupling dense 3D mesh so it takes up the least amount of space. The inductive coupling ring swaps spots with the capacitive coupling mesh between 64 and 256 cores because the number of inductive coupling links only doubles instead of increasing by a factor of four.

### **5.1.5 Overall**

If the manufacturing process can be supported and chip area is not the most important design criteria, TSVs would work well for connecting chip layers. When a wireless interconnect is required, the decision comes down to power, performance, and chip area. The inductive coupling sparse 3D mesh consumes the most energy of all of the wireless architectures, but it uses the least amount of chip area and has the lowest packet latency for typical workloads. Otherwise, the inductive coupling ring is more ideal for chip area constrained systems while the inductive coupling dense 3D mesh networks would be suitable for power constrained systems.

### **5.2. *Future Work***

In addition to the work presented here, there are a few areas that could benefit from further research. The first is a broader comparison of emerging technologies such as photonic and RF interconnects. Their energy consumption and latency characteristics can be applied to the simulator to yield performance and energy results that can be compared to the established metrics for the technologies covered in this work. This would enable a comprehensive exploration of the performance and energy consumption for these emerging technologies. Similarly, small world networks can be applied to the technologies to measure the impacts on energy and performance, which would also provide insight into the benefits and disadvantages of the architecture. Another area of research that could be expanded upon is the sparse 3D mesh. The sparse 3D mesh architecture can be scaled to higher core counts and different network configurations could be explored. The sparse 3D mesh could also be applied to the TSV mesh and reduced number of TSV connections to see the impact it has on power and performance.

A more comprehensive investigation of the sparse 3D mesh may reveal further applications for the architecture.

## References

- [1] Magarshack, P. and Paulin, P.G., "System-on-chip beyond the nanometer wall," *Design Automation Conference, 2003. Proceedings*, pp. 419-424, June 2003.
- [2] Ho, R., Mai, K.W. and Horowitz, M.A., "The future of wires," *Proceedings of the IEEE*, vol. 89, no. 4, pp. 490-504, Apr 2001.
- [3] Pande, P.P., Grecu, C., Jones, M., Ivanov, A. and Saleh, R., "Performance evaluation and design trade-offs for network-on-chip interconnect architectures," *Computers, IEEE Transactions on*, vol. 54, no. 8, pp. 1025-1040, Aug 2005.
- [4] Feero, B.S. and Pande, P.P., "Networks-on-Chip in a Three-Dimensional Environment: A Performance Evaluation," *Computers, IEEE Transactions on*, vol. 58, no. 1, pp. 32-45, Jan 2009.
- [5] M. Koyanagi, H. Kurino, L. Kang-Wook, K. Sakuma, N. Miyakawa and H. Itani, "Future system-on-silicon LSI chips," *Micro, IEEE*, vol. 18, no. 4, pp. 17-22, Jul 1998.
- [6] K. Banerjee, S. J. Souri, P. Kapur and K. C. Saraswat, "3-D ICs: a novel chip design for improving deep-submicrometer interconnect performance and systems-on-chip integration," *Proceedings of the IEEE*, vol. 89, no. 5, pp. 602-633, May 2001.
- [7] R. S. Patti, "Three-Dimensional Integrated Circuits and the Future of System-on-Chip Designs," *Proceedings of the IEEE*, vol. 94, no. 6, pp. 1214-1224, June 2006.



- [8] W. R. Davis, J. Wilson, S. Mick, J. Xu, H. Hua, C. Mineo, A. M. Sule, M. Steer and P. D. Franzon, "Demystifying 3D ICs: the pros and cons of going vertical," *Design Test of Computers, IEEE*, vol. 22, no. 6, pp. 498-510, Nov 2005.
- [9] J. Ouyang, J. Xie, Poremba, M. and Y. Xie, "Evaluation of Using Inductive/Capacitive-coupling Vertical Interconnects in 3D Network-on-chip," in *Proceedings of the International Conference on Computer-Aided Design*, San Jose, California, IEEE Press, 2010, pp. 477-482.
- [10] Z. Xu and J.-Q. Lu, "Through-Silicon-Via Fabrication Technologies, Passives Extraction, and Electrical Modeling for 3-D Integration/Packaging," *Semiconductor Manufacturing, IEEE Transactions on*, vol. 26, no. 1, pp. 23-34, Feb 2013.
- [11] Miura, N., Ishikuro, H., Niitsu, K., Sakurai, T. and Kuroda, T., "A 0.14pJ/b Inductive-Coupling Inter-Chip Data Transceiver with Digitally-Controlled Precise Pulse Shaping," in *Solid-State Circuits Conference, 2007. ISSCC 2007. Digest of Technical Papers. IEEE International*, 2007, pp. 358-608.
- [12] Lim, E., Yoshikawa, T., Kim, T.T.-H and M. T. L. Aung, "Design of Simultaneous Bi-Directional Transceivers Utilizing Capacitive Coupling for 3DICs in Face-to-Face Configuration," *Emerging and Selected Topics in Circuits and Systems, IEEE Journal on*, vol. 2, no. 2, pp. 257-265, June 2012.
- [13] R. Morris, A. Kodi and A. Louri, "3D-NoC: Reconfigurable 3D photonic on-chip interconnect for multicores," in *Computer Design (ICCD), 2012 IEEE 30th International Conference on*, 2012.

- [14] S. Deb, A. Ganguly, K. Chang, P. Pande, B. Beizer and D. Heo, "Enhancing performance of network-on-chip architectures with millimeter-wave wireless interconnects," in *Application-specific Systems Architectures and Processors (ASAP), 2010 21st IEEE International Conference on*, 2010, pp. 73-80.
- [15] A. Ganguly, K. Chang, S. Deb, P. Pande, B. Belzer and C. Teuscher, "Scalable Hybrid Wireless Network-on-Chip Architectures for Multicore Systems," *Computers, IEEE Transactions on*, vol. 60, no. 10, pp. 1485-1502, Oct 2011.
- [16] M. P. Yuvaraj, *Design Trade-offs for reliable On-Chip Wireless Interconnects in NoC Platforms*, Rochester Institute of Technology, 2014.
- [17] A. More and B. Taskin, "Simulation Based Feasibility Study of Wireless RF Interconnects for 3D ICs," in *VLSI (ISVLSI), 2010 IEEE Computer Society Annual Symposium on*, 2010, pp. 228-231.
- [18] Y. Take, H. Matsutani, D. Sasaki, M. Koibuchi, T. Kuroda and H. Amano, "3D NoC with Inductive-Coupling Links for Building-Block SiPs," *Computers, IEEE Transactions on*, vol. 63, no. 3, pp. 748-763, March 2014.